mGBP2 engages Galectin-9 and Cytoskeleton-associated Protein 4 for immunity against *Toxoplasma gondii*

Elisabeth Kravets[1], Gereon Poschmann[2], Sebastian Hänsch[3], Stefanie Weidtkamp-Peters[3], Daniel Degrandi[1], Kai Stühler[2,4], Klaus Pfeffer[1*].

[1] Institute of Medical Microbiology and Hospital Hygiene, Heinrich Heine University Düsseldorf, Düsseldorf, Germany

[2] Institute of Molecular Medicine, Proteome Research, Medical Faculty and University Hospital, Heinrich-Heine-University Düsseldorf, Germany

[3] Center of Advanced Imaging, Heinrich Heine University Düsseldorf, Düsseldorf, Germany

[4] Molecular Proteomics Laboratory, Biological and Medical Research Centre (BMFZ), Heinrich-Heine-University Düsseldorf, Düsseldorf, Germany

Corresponding author:

Prof. Dr. Klaus Pfeffer
Institute of Medical Microbiology and Hospital Hygiene
Heinrich Heine University Düsseldorf
Universitätsstr. 1
D-40225 Düsseldorf
Phone: +49 211 81 12459
e-mail: klaus.pfeffer@hhu.de

Author Contributions

EK designed and performed most experiments; GP and KS performed and analyzed the mass spectrometry data; SH and SWP performed STED microscopy and analysis. DD and KP designed and supervised the study. EK, DD and KP wrote the paper. All authors contributed in writing, discussing and editing of the manuscript.

Competing Interest Statement:

None of the authors has a financial interest related to this work

Classification

Biological Sciences, Immunology and Inflammation

Keywords:

Guanylate-binding-proteins, Toxoplasma gondii, Host-Pathogen interaction

This PDF file includes

Main Text

Figures 1 to 6

Supplementary Figures S1 to S10

Abstract

Guanylate binding proteins (GBPs) are large interferon-inducible GTPases, executing essential host defense activities against *Toxoplasma gondii,* an invasive intracellular apicomplexan protozoan parasite of global importance. *T. gondii* establishes a parasitophorous vacuole (PV) which shields the parasite from the host's intracellular defense mechanisms. Murine GBPs (mGBPs) recognize *T. gondii* PVs and assemble into supramolecular mGBP homo- and heterocomplexes that are required for the disruption of the membrane of PVs eventually resulting in the cell-autonomous immune control of vacuole-resident pathogens. We have previously shown that mGBP2 plays an important role in *T. gondii* immune control. Here, in order to unravel mGBP2 functions, we report Galectin-9 (Gal9) and cytoskeleton-associated protein 4 (Ckap4) as critical mGBP2 interaction partners engaged for immunity to *T. gondii*. Interestingly, Gal9 and Ckap4 also accumulate and colocalize with mGBP2 at the *T. gondii* PV. Furthermore, we could prove the requirement of Gal9 and Ckap4 for growth control of *T. gondii* by CRISPR/Cas9 mediated gene editing. These discoveries clearly indicate that mGBP2 engages Gal9 and Ckap4 and that Gal9 and Ckap4 are critical factors for the mGBP2 coordinated cell autonomous host defense mechanism against *T. gondii*.

Significance Statement

We have previously shown that mGBP2 is an essential IFNγ induced protein for defense against *Toxoplasma gondii* infection. mGBP2 is rapidly recruited to the parasitophorous vacuole (PV) of intracellular *T. gondii* and is required for the rupture and/or permeabilization of the PV membrane. Subsequently mGBP2 attacks the parasite membrane. Up to now, no data about other mGBP2 interaction partners and their molecular requirement for *T. gondii* control has been made available.

Here, we have identified Gal9 and Ckap4 as interacting proteins of mGBP2. Gal9 and Ckap4 are essential in the mGBP2 mediated attack of the *T. gondii* PV. Both proteins localize at the *T. gondii* PV in close association with mGBP2, as shown by state-of-the-art super resolution microscopy. In addition, *T. gondii* growth cannot be controlled anymore in Gal9 and Ckap4 deficient cell lines, comparable to mGBP2 deficient cells,.

62 Thus, we have identified novel effector proteins in the intricate cell autonomous immune machinery against intracellular

63 pathogens.

64

65 **Introduction**

66 Subsequent to innate immune sensing of pathogens via pattern recognition receptors, production of interferons (IFN)
67 is a key prerequisite for the activation of cell-autonomous immunity, which is essential for the immediate restriction of
68 microbial replication (1, 2). IFN-γ signaling induces the expression of hundreds of interferon-stimulated genes (ISGs)
69 (3-5), which essentially contribute to innate and adaptive immune responses in immune and nonimmune cells (6, 7).
70 Very prominent among IFN-γ ISGs are the members of several families of interferon-inducible GTPases such as the
71 65- to 73-kDa dynamin-related guanylate-binding proteins (GBPs) (8, 9) and the 45-kDa immunity-related GTPases
72 (IRGs) (10, 11). Human (hGBPs) and murine GBPs (mGBPs) families consist of seven (hGBP1 to hGBP7) and eleven
73 (mGBP1 to mGBP11) members, respectively, which are strongly upregulated in response to IFN-γ (12-14). GBPs
74 characteristically exhibit various cellular functions encompassing antiparasitic, antiviral, and antibacterial activity, as
75 well as inhibitory effects on cell proliferation and tumor suppression (15-26).

76 GBPs display a characteristic multidomain architecture including a large catalytic GTPase (G) domain and a C-terminal,
77 helical domain (8, 27-33). Various mGBPs such as mGBP1, mGBP2, and mGBP7 are especially important effector
78 molecules for the resistance against *Toxoplasma gondii*, an intracellular apicomplexan protozoan parasite of global
79 importance (16, 25, 34-39). After the active invasion of host cells, *T. gondii* forms a nonfusogenic cytoplasmic
80 membranous structure called the parasitophorous vacuole (PV) in which the parasite efficiently replicates (37, 40, 41).
81 mGBPs are intricately involved in IFN-γ induced growth restriction and killing of the *T. gondii* in murine macrophages,
82 fibroblasts and astrocytes (16, 20, 25, 36, 38, 42). In order to execute their antimicrobial function, mGBPs can
83 specifically associate with pathogen containing compartments of intracellular microbes which encompass pathogen-
84 containing vacuoles (PCVs) as well as viral replication compartments (20, 25, 36, 43-45), resulting in the innate immune
85 detection and cell-autonomous clearing or of PCV-resident pathogens (22, 25, 38, 46). After IFN-γ induction, mGBP2
86 molecules assemble in vesicle like structures (VLS) in the cytoplasm and, after *T. gondii* entry into the host cell, mGBP2
87 attacks the PV membrane (PVM) in orchestrated, supramolecular complexes, ultimately promoting the destruction of
88 PVMs (36, 38). This stage is followed by recruitment of mGBP2 to the plasma membrane of the intracellular parasite,
89 which in turn likely leads to its destruction (38). Multiparameter fluorescence image spectroscopy (MFIS) revealed that

90 mGBP2, on a molecular level, can form homomultimers or heteromultimers with mGBP1, mGBP3 and, to a lesser
91 extent, with mGBP5 within VLS and at the PVM (38). For PV membrane interactions, isoprenylation / farnesylation
92 and/or hydrophobic moieties in the C-terminus of the GBPs are essential (25, 31, 32, 38, 47). Eventually, especially
93 mGBP2 and mGBP7, can be found localized at the parasite cell membrane and inside the targeted parasite (25, 38)
94 probably also interfering with the integrity of *T. gondii* membranes. Importantly, inactivation of mGBP1, mGBP2, or
95 mGBP7 in mice has been shown to result in a vastly impaired resistance to infections with type II *T. gondii* (25, 36).

96 Galectins are a family of lectins characterized by a carbohydrate recognition domain (CRD) with β-galactoside-binding
97 ability (48). Galectins are nucleocytoplasmic, can also be exported from cells through a poorly defined unconventional
98 secretion pathway (49) and can bind directly to bacteria thereby mediating antibacterial effects and modifying
99 inflammatory signaling events (50). Presently, 15 galectin members have been identified in mammals (51).
100 Immunomodulatory effects of galectins include recruitment of immune cells to the site of infection, promotion of
101 neutrophil function, and stimulation of the bactericidal activity of infected neutrophils and macrophages (48). Previously
102 it has been shown that Gal3 can bind *T. gondii* glycophosphatidylinositols and might be a co-receptor presenting GPIs
103 to TLRs on macrophages (52). Cytoplasmic galectins fulfill functions in several cellular programs including cell growth
104 and apoptosis (53). Through binding to multivalent carbohydrates, galectins can multimerize and thereby cluster these
105 surface glycoconjugates resulting in changes in cell migration, receptor endocytosis and various other cellular events
106 (54, 55). Glycans are largely restricted to the luminal face but absent from the cytosolic face of intracellular vesicles. If
107 vesicular damage occurs, luminal glycans are exposed to the cytosolic milieu, where they can be recognized by
108 galectins (56, 57) . Furthermore, vacuolar instability of bacterial PCVs is recognized by host β-galactoside-binding
109 proteins of the galectin family (50, 58). Intracellular galectins can serve as danger receptors and can promote autophagy
110 of the invading pathogen (59).

111 The aim of this study was to explore the molecular interaction(s) which enable mGBP2 to control *T. gondii* replication.
112 By employing immunoprecipitation (IP) followed by mass spectrometry (MS) analysis, we have identified novel
113 interaction partners of mGBP2 such as galectin-9 (Gal9) and cytoskeleton-associated protein 4 (Ckap4). Furthermore,
114 we demonstrate that the inactivation of either Gal9 or Ckap4 impairs the cell autonomous IFN-γ induced immune control
115 of *T. gondii* replication.

116

117 **Results**

118 *Identification of Gal9 and Ckap4 as mGBP2 interaction partners by IP and MS*

119 Previously, we could show that mGBP2 interacts with itself and other mGBP family members forming homo- and
120 heteromultimers, respectively, in VLS and at the *T. gondii* PVM (38). For a profound understanding of the functions of
121 mGBP2 in *T. gondii* infection, we searched for other interaction partners of mGBP2. To this end, mGBP2$^{-/-}$ murine
122 embryonic fibroblasts (MEFs)(36) expressing HA-tagged mGBP2 were constructed, stimulated with IFN-γ, and either
123 infected with the type II strain *T. gondii* ME49 or left uninfected. An HA-tag specific IP was performed (Fig.S1) followed
124 by MS based quantitative protein analysis (Fig.1). mGBP2$^{-/-}$ MEFs transduced with an empty expression vector served
125 as negative controls.

126 Statistical analysis revealed that 148 proteins were co-purified with HA-mGBP2 from the uninfected and 294 proteins
127 from the *T. gondii* infected cells. Besides the bait protein mGBP2, further members of the mGBP family were enriched
128 as prey proteins. Among them, a clear co-purification of mGBP1 and mGBP5 which previously were independently
129 identified by MFIS as mGBP2 interacting members, could be observed in uninfected and infected HA-mGBP2
130 expressing MEFs (mGBP1 enrichment factor > 185 in both experimental conditions, mGBP5 enrichment factor 4.8 from
131 uninfected and 15.1 from infected cells) (Fig.1), verifying the reliability of the co-IP and MS analysis. Furthermore,
132 Ckap4 showed up to be specifically enriched in mGBP2 immunoprecipitation experiments.

133 Members of the galectin family were significantly enriched in IPs from *T. gondii* infected cells. From the list of potential
134 mGBP2 interactors, Gal9 was analyzed further since Gal9 was found significantly enriched in IP samples from type II
135 *T. gondii* ME49 infected cells (Fig.1) and interestingly a role for several other galectin family members had already been
136 proposed in microbial infections (51). Furthermore, Ckap4 showed a high enrichment factor (uninfected: 9.2 / *T. gondii*
137 infected: 14) comparable to the known mGBP2 interacting proteins mGBP1 and mGBP5 (Fig.1).

138 To validate and characterize the interactions of Gal9 and Ckap4 with mGBP2 in detail, mCherry-fused proteins of Gal9
139 or Ckap4 were co-expressed with full-length mGBP2 or with mGBP2 truncation mutants containing the GTP-binding
140 domain only (G), the G-domain and the middle domain (GM) or the C-terminal effector domain (E) (31, 36). These cell
141 lines were infected with *T. gondii* followed by co-IP. Using this approach, we could prove the interaction of mGBP2 with

142 Gal9 and Ckap4 and could determine a crucial function of the E-domain of mGBP2 for the interaction with Gal9 and
143 Ckap4 (Fig.2).

144

145 *Subcellular localization of Gal9 and Ckap4 and recruitment to the T. gondii PV*

146 In a next step, the colocalization of mGBP2 and Gal9 or Ckap4 at the PVM of *T. gondii* was determined by confocal
147 (Fig.S2) and Stimulated Emission Depletion (STED) microscopy (Fig.3). Doubly transduced mGBP2$^{-/-}$ MEFs
148 coexpressing GFP-mGBP2 with either mCherry-Gal9 or mCherry-Ckap4 were prestimulated with IFN-γ and infected
149 with *T. gondii* ME49 (Fig.3, Fig.S2). GFP-mGBP2 and mCherry-mGBP2 coexpressing MEFs served as a positive
150 control in STED microscopy colocalization experiments (Fig.S3). A distinctive colocalization or close association
151 between mGBP2 and Gal9 and between mGBP2 and Ckap4 could be observed at the PVM already 2 h after infection.
152 Interestingly, mCherry-Gal9 partly colocalized in GFP-mGBP2 containing VLS in uninfected MEFs, whereas a
153 colocalization of mCherry-Ckap4 and GFP-GBP2 containing VLS could hardly be visualized by confocal microscopy
154 (Fig.S4). Furthermore, 5-6 h after infection, different stages of recruitment and accumulation of mGBP2 and its
155 interaction partners at the PVM were observed (Fig.S2). Eventually, Gal9 and mGBP2 could be found to be located
156 together within the intermembranous space of the PV and eventually within the cytosol of the parasite (Fig.S2). These
157 results indicate that Gal9 and Ckap4 are interacting and acting together with mGBP2 and suggest that Gal9 and Ckap4
158 are intricately involved into the cell autonomous immunity mediated by mGBP2.

159

160 *Recruitment of mGBP2 to the T. gondii PV in Gal9 or Ckap4 deficient cells.*

161 Next, the roles of Gal9 and Ckap4 for the recruitment of mGBP2 to the *T. gondii* PV was analyzed. For this purpose,
162 the *gal9* gene as well as the *ckap4* gene were inactivated applying CRISPR/Cas9 gene editing. The inactivation of Gal9
163 and Ckap4 in different clonal NIH 3T3 fibroblast cell lines was confirmed by sequencing of the targeted gene loci and,
164 additionally, either by Surveyor nuclease assay and WB for Gal9 (Fig.S5) or by WB analysis with a specific antibody
165 against Ckap4 (Fig.S6). No difference in *T. gondii* infection rates could be detected between WT or Gal9- or Ckap4
166 inactivated fibroblast cell lines (Fig.S7). Interestingly, a significant reduction in the recruitment efficiency of mGBP2 2 h

167 after infection was observed in the absence of Gal9 or Ckap4 in the targeted fibroblast cell lines (Fig.4). Recruitment of
168 mGBP2 could be restored after reconstitution of the fibroblasts with either mCherry-Gal9 or mCherry-Ckap4 (Fig.4).
169 Interestingly, the recruitment of Gal9 was also reduced in mGBP2 deficient MEFs, whereas the co-localization of Ckap4
170 at the *T. gondii* PVM was not affected by the lack of mGBP2 (Fig.4, Suppl. Fig.8). These data indicate that the
171 recruitment of mGBP2 to the *T. gondii* PVM is more efficient in the presence of Gal9 and Ckap4.

172

173 *T. gondii replication control by Gal9 and Ckap4*

174 The course of *T. gondii* infection in cells deficient for Gal9 and Ckap4 was investigated in the next step. To address the
175 question whether Gal9 and / or Ckap4 contribute to cell autonomous immunity against *T. gondii*, Gal9- and Ckap4-
176 deficient fibroblast cell lines were stimulated with IFN-γ and infected with *T. gondii* (ME49) and the replication of the
177 parasite was monitored. First, it was determined whether the inactivation of Gal9 or Ckap4 leads to increased or
178 decreased infection rates in the targeted cell lines compared to wildtype cells. However, the number of *T. gondii*
179 parasites detected in the gene edited cell lines compared to wildtype fibroblasts did not differ 2 h post infection (Fig.S7).
180 Interestingly, a significant increase in *T. gondii* replication could be observed in fibroblasts harboring an inactivation of
181 Gal9 or Ckap4 as determined by quantification of the number of *T. gondii* rosettes and single parasites 22 h after
182 infection (Fig.5, Fig.S9). As a specific control and to verify the specificity of the CRISPR/Cas9 gene inactivation of Gal9
183 and Ckap4, Gal9- and Ckap4- deficient cell clones were reconstituted by transduction with mCherry-Gal9 and mCherry-
184 Ckap4 expression constructs, respectively. Importantly, Toxoplasma replication in the reconstituted fibroblasts was
185 inhibited comparably to WT cells (Fig.6, Fig.S9). These results clearly indicate an important role for Gal9 and Ckap4 in
186 controlling the intracellular replication of the parasite and suggest that mGBP2, Gal9 and Ckap4 function as
187 supramolecular complexes in the defense against intracellular pathogens.

188

189 **Discussion**

190 mGBP2 provides cell-autonomous immunity to the intracellular PV resident parasite *T. gondii* (31, 36, 38, 44, 60).
191 Although it has been shown that mGBPs translocate to PVs, form supramolecular complexes, attack the membrane of
192 the parasite itself, and, consecutively, restrict replication of the intracellular pathogen, the molecular mechanisms by
193 which mGBPs control the parasite inside the host cell remain largely elusive. Here we propose two novel interaction
194 partners of mGBP2, Gal9 and Ckap4, which play a critical role with respect to the recruitment and the antiparasitic
195 function of mGBP2 in the context of cell-autonomous defense against *T. gondii* (for a schematic overview see Fig.S10).

196 Previously, it was shown that Gal8 colocalizes with mGBP2 positive *Salmonella spp*. in unprimed bone marrow derived
197 macrophages (BMDMs) (61). It was proposed that Gal8 monitors endosomal and lysosomal integrity and detects
198 bacterial invasion of the cytosol by *Listeria* spp. or *Shigella spp.*, serving as a versatile receptor for vesicle-damaging
199 pathogens (61). Interestingly, it was also reported that Gal3, as a member of the Galectin family, and mGBP2 form
200 protein complexes, which associate with vacuoles harboring secretion system-competent *Legionella pneumophila* and
201 *Yersinia pseudotuberculosis* bacteria in response to vacuolar damage (62). In this study we show that Gal9 interacts
202 and colocalizes with mGBP2 in IFN-γ stimulated MEFs and NIH 3T3 cells in VLS. Based on its structural organization,
203 Gal9 belongs to the tandem-repeat type galectins containing two distinct but homologous CRDs (N-CRD and C-CRD)
204 covalently connected by a linker peptide (48, 59). Recruitment of Gal9 to the *T. gondii* PV has not been described
205 previously. Furthermore, Gal9 could not only be found at the PVM but also within the intermembranous space between
206 the PVM and the *T. gondii* plasma membrane as well as in the cytosol of the parasites together with mGBP2 approx.
207 5-6 h post-infection. This indicates that Gal9 and mGBP2 might recruit to the PVM of *T. gondii* in preformed complexes.
208 Mechanistically, a series of events involving mGBP/IRG mediated PVM indentation, PVM vesiculation/disruption, and
209 parasite plasma membrane stripping and denudation, leading ultimately to degradation of the parasite, is proposed by
210 us and others as hallmarks for intracellular *T. gondii* elimination (38, 63, 64). It can be suggested that poreforming or
211 denudating activity of these IFN-γ induced GTPases allows Gal9 to transmigrate through the PVM and to recognize β-
212 galactosides on the inner leaflets of the PVM and the parasite, labeling the parasite for further degradation processes.
213 Parasite glycoconjugates play important roles in host cell invasion, and specific interactions between host galectins and
214 parasite glycoconjugates are considered to be critical for pathogen recognition (55). Interestingly,

215 glycosylphosphatidylinositols (GPIs) of *T. gondii* (65) have been shown to be ligands of human Gal3 whereby both
216 glycan and lipid moieties participate in the association of *T. gondii* GPIs with Gal3 (52). In this context, Gal3, -8, and -9
217 bind to host glycans in the luminal side of lysed phagosomes or permeated pathogen vacuoles (66). Intracellular Gal3
218 was characterized as a sensor of vacuolar rupture that occurs when bacteria such as *Shigella flexneri* or *Salmonella*
219 *enterica* serovar Typhimurium actively enter the host cell cytosol (58, 67). Moreover, *S. flexneri* IpaH9.8 labels mGBP2
220 for degradation (68). Gal3, -8 and -9 were also shown to associate with Salmonella-containing vacuoles (SCV) (61, 69,
221 70). Here we show that Gal9 is required for the control of the parasite *T. gondii*.

222 Functionally, the recruitment of mGBP2 to the PVM was reduced in Gal9- inactivated cells and vice versa; the
223 recruitment of Gal9 to the PVM was reduced in mGBP2 deficient cells. In accordance, significantly fewer Salmonella
224 were targeted by Gal8 in Gbp^{chr3} KO BMDMs than in wild-type BMDMs (71). Also, the delivery of mGBP1 and mGBP2
225 to Legionella-containing vacuoles (LCV) or Yersinia-containing vacuoles is substantially diminished in Gal3- and, to a
226 lesser extent, Gal8-deficient IFN-γ–primed iBMDM (62). In Salmonella-infected cells, SCV rupture and Gal3 recruitment
227 was followed by a rapid and massive recruitment of hGBP1 (67). Interestingly, a specific polybasic protein motif (PBM:
228 KMRRRK) was identified for hGBP1 which is sufficient to drive significant targeting of hGBP1 to *S. flexneri* recognizing
229 exposed glycans from disrupted, bacteria containing, endosomes. Deletion of the PBM-motive leads to substantially
230 reduced colocalization between Gal3-marked vacuoles and hGBP1 (72). mGBP2 lacks such a C-terminal PBM.
231 Nevertheless, the interaction with Gal9 appears to be mostly dependent on the C-terminal domain of mGBP2. Rab GDP
232 dissociation inhibitor α (RabGDIα) acts as a suppressor of the mGBP2-Irga6 axis, hereby the lipid-binding activity of
233 RabGDIα is critical for IFN-γ–induced mGBP2-dependent cell-autonomous immunity against ME49 *T. gondii*. RabGDIα
234 deficiency is accompanied by increased recruitment of mGBP2 and Irga6 to the parasite in MEFs and macrophages
235 and results in enhanced IFN-γ–mediated *T. gondii* clearance *in vitro* and *in vivo* (73). These studies suggest on the
236 one hand GBPs as escorts for distinct anti-pathogenic factors en route to PVs, on the other hand that the recruitment
237 of galectins and GBPs to the PVs might be mutually dependent as part of a coordinated host defense program. This is
238 supported by the significantly increased *T. gondii* proliferation in IFN-γ stimulated Gal9 knock out 3T3 fibroblasts 22h
239 post-infection indicating an important role of Gal9 in cell-autonomous *T. gondii* elimination. In contrast, IFN-γ–primed
240 $Gal3^{-/-}$ BMDMs restricted Yersinia and Legionella bacterial growth, similar to WT BMDMs (62).

241 Thus, it might be speculated that the recognition of the lysed PV by Gal9 initiates the uptake of the parasite into
242 autophagosomes or other degradation pathways as it was described for *Salmonella*, where GBPs promote LC3
243 recruitment via Gal8 (71). Interestingly, *T. gondii* infected Gal3$^{-/-}$ mice develop reduced inflammatory responses in
244 many organs (74) and succumb to an intraperitoneal infection with *T. gondii* associated with a deficient influx of
245 neutrophils and macrophages into the peritoneal cavity (75). The function of Gal9 might be the non-redundant to Gal3
246 and Gal8 in parasitic degradation processes which will be addressed in the future in a Gal9-gene deficient mouse line.

247 Ckap4 and mGBP2 can colocalize at the PVM of *T. gondii* where Ckap4 binds to the C-terminal part of mGBP2. Ckap4,
248 also known as p63, CLIMP-63, or ERGIC-63, is a 63 kDa, reversibly palmitoylated and phosphorylated, type II integral
249 transmembrane (TM) protein. Ckap4 was originally identified as a resident of the endoplasmic reticulum (ER)/Golgi
250 intermediate compartment (ERGIC) (76) linking the ER to microtubules (77). There is also steadily accumulating
251 evidence for diverse roles for Ckap4 localized outside the ER, including data demonstrating functionality of Ckap4 as a
252 cell surface receptor for Dickkopf1-cytoskeleton-associated protein 4 (DKK1) (78) and other ligands (79, 80) resulting
253 in increased nuclear abundance of Ckap4 in response to the antiproliferative factor (APF) (81). Ckap4 must be
254 palmitoylated to traffic to the cell surface (82).

255 After active invasion and sequestration in PVs, intracellular *T. gondii* parasites initiate the reorganization of the ER and
256 recruit the microtubule organizing center and other factors of the host cell cytoskeleton to PVs (83) to obtain nutrition
257 sources (84). Microtubules of the host, which are loaded with LDL cholesterol (85) form a connection with the PV and
258 are anchored via the "Dense Granule" protein GRA7 of *T. gondii*, organizing a tubulo-vesicular network (TVN) (86).
259 When localized to the ER, a major function of Ckap4 is to anchor rough ER to microtubules, organizing the overall
260 structure of ER with respect to the microtubule network. Vacuole formation and trafficking within the cytoplasm of
261 eukaryotic cells is dependent upon the cytoskeleton and cytoskeletal motors (87-89). Therefore, it might not to be
262 surprising that PCV are tightly associated with cytoskeletal components and that modulation of the cytoskeleton is a
263 key process required for vacuole formation. Intimate interactions between *T. gondii* and host microtubules were shown
264 to result in suppression of cell division and/or cause a mitotic defect, thus providing a larger space for parasite
265 duplication (90). Also, interference with the cytoskeleton has been shown to be required for expansion of Salmonella
266 and Chlamydia PCVs (91, 92). The regulation of the cytoskeleton by IFN-γ is of relevance in physiological and

267 pathophysiological processes, including cell migration, invasion, proliferation, defense against pathogens, and barrier
268 function (93-98) and hGBP1 has been shown to be involved into the regulation of these cellular processes in response
269 to IFN-γ (15, 17, 98-100). Interestingly, hGBP1 has been proposed to be involved in rearrangements of the cytoskeleton
270 specifically mediating IFN-γ induced defense mechanisms, where actin-remodeling was dependent on the
271 oligomerization and the GTPase activity of hGBP1 (101). Salmonella and Chlamydia PCVs are surrounded by a network
272 of F-actin and other cytoskeletal components that provide structural support for the PCVs of both these pathogens as
273 treatment with F-actin polymerisation inhibitors leads to the loss of integrity (92, 102, 103). Thus, Ckap4 might inhibit
274 the establishment of the intracellular parasitic survival niche and this is involved into the replication control of *T. gondii*.
275 The molecular function of Ckap4 in the mGBP2 complex and the putative ability of Ckap4 to associate with other
276 members of the GBP family have to be addressed in the future. The findings of this study indicate that mGBP2 acts as
277 a scaffold organizing the cell autonomous immunity in concert with Gal9 and Ckap4 and thus extends the understanding
278 of molecular host responses in the control of intracellular parasites.

279 **Materials and Methods**

280 *Expression Constructs.*

281 The WT ORF of mGBP2 (NCBI accession numbers: mGBP-2, NM_010260.1) was cloned either into the pWPXL
282 plasmid (Trono lab) as N-terminal GFP-fusion constructs or into the pWPI Plasmid (Trono lab) in frame with a N-terminal
283 HA-tag. For the cloning of mCherry constructs (36), the pWPXL plasmid was modified by exchanging of the gene for
284 GFP by the gene for mCherry (38). mRNA was isolated from freshly prepared WT MEFs prestimulated with IFN-γ and
285 infected with *T. gondii*. The ORFs of Galectin 9 (NM_010708.2) and Ckap4 (NM_175451.1) were amplified by PCR and
286 then cloned into the modified pWPXL plasmid as N-terminal mCherry-fusion constructs (38). The lentiviral envelope
287 vector pLP/VSVG (Invitrogen) and the packaging vector psPAX2 (Trono lab) were used for the lentiviral genetic transfer.

288 *Cell culture and transduction.*

289 NIH 3T3 fibroblasts and MEFs were cultured in Dulbecco's modified Eagle's medium (DMEM, Invitrogen/Gibco)
290 supplemented with 10% (v/v) heat-inactivated low endotoxin fetal bovine serum (FBS, Cambrex), 100 U/ml penicillin,
291 100 µg/ml streptomycin, 2 mM L-glutamine (Biochrom) and 0.05 mM β-mercaptoethanol (Invitrogen/Gibco). Human

292 foreskin fibroblasts (HS27, ATCC CRL-1634) were hold in culture in Iscove's Modified Dulbecco's Medium (IMDM,
293 Invitrogen/Gibco) with the same supplementations. 293FT cells were cultivated in DMEM supplemented with 10% FBS,
294 100 U/ml penicillin, and 100 µg/ml streptomycin. All recombinant lentiviruses were produced by transient transfection
295 of 293FT cells according to jetPRIME® transfection protocol (Polyplus, New York City) (38). NIH 3T3 cells and MEFs
296 were seeded in 24 well plates (Corning Incorporated, Germany) and transduced with 600 µl of lentivirus with 25 µg
297 Polybrene (Merck Millipore, Germany). After 5 h of incubation medium was changed. The transduction efficacy was
298 analyzed by flowcytometry. Subsequently, only GFP or double GFP and mCherry positive cells were sorted and
299 cultivated.

300 *In Vitro Passage of Toxoplasma gondii.*

301 Tachyzoites from *T. gondii* strain ME49 were maintained by serial passage in confluent monolayers of HS27 cells. After
302 infection of fibroblasts, parasites were harvested and passaged as described previously (16).

303 *Infection of murine MEFs with T. gondii.*

304 Cells were stimulated with 200 U/mL IFN-γ (R&D Systems, Minneapolis, MN) 16 h before infection. For
305 immunofluorescence, NIH 3T3 fibroblasts and MEFs were cultured in 24-well plates (Falcon, BD
306 Biosciences, Germany) on cover slips (ø 13 mm, VWR International, Germany) and inoculated with freshly harvested
307 T. gondii at a ratio of 50:1. To remove extracellular parasites, cells were washed with PBS.

308 *Pull-Down and co-immunoprecipitation analysis of mGBP2*

309 For pull down experiments, mGBP2$^{-/-}$ MEFs reconstituted with HA-mGBP2 were used. mGBP2$^{-/-}$ MEFs transduced with
310 the empty pWPI vector were used as control cells. Cells were then stimulated with IFN-γ for 16 h, infected with the *T.*
311 *gondii* strain ME49 for 2 h or left uninfected, subsequently lysed and postnuclear supernatants were incubated o/n with
312 monoclonal mouse anti-HA- antibody coupled to agarose beads (clone HA-7, Sigma-Aldich, USA) at 4°C. IP probes
313 were subjected to silver staining and to Western Blotting. Blots were stained with the mGBP2-specific antiserum
314 (Eurogentec), mouse α-GFP (clones 7.1 and 13.1, Roche, Switzerland) and rabbit αHA (polyclonal, Sigma-Aldich,
315 USA) antibodies. For IP experiments, postnuclear supernatants of mGBP2$^{-/-}$ MEFs reconstituted either with WT GFP-
316 mGBP2 or GFP-fused truncated mutants mutants or just transduced with a GFP expressing vector, as an appropriate

317 control and coexpressing mCherry fused with Gal9 or Ckap4 or just the mCherry protein, were incubated o/n with RFP-
318 Trap® or GFP-Trap® beads (ChromoTek GmbH, Germany) at 4°C. IP probes were subjected to Western Blotting. Blots
319 were stained with the mouse α-GFP or α-mCherry (Clontech, EU) antibodies.

320 *MS Analysis of interaction partners of mGBP2*

321 A label-free mass spectrometry, based quantification approaches enabled by a highly reproducible and stable LC-
322 MS/MS system was chosen for a quantitative analysis of the mGBP2 interactome. Six individual replicates of co-
323 immunoprecipitation samples per group (HA-mGFP2, control-vector, HA-mGFP2 + ME49 and control-vector + ME49)
324 were prepared from transfected IFNγ stimulated mGBP2$^{-/-}$ MEFs (see above). Samples were prepared for mass
325 spectrometric analysis essentially as described elsewhere (104). Briefly, proteins were stacked into an acrylamide gel
326 (about 4 mm running distance), subjected to silver staining, de-stained, reduced and alkylated and digested with trypsin.
327 Resulting peptides were extracted from the gel and approximately 500 ng peptides prepared in 0.1% trifluoroacetic acid
328 for liquid chromatography and mass spectrometric analysis.

329 First, peptide samples were separated on an UltiMate 3000 RSLCnano chromatography system (Thermo Fisher
330 Scientific). Peptides were initially trapped on a 2 cm long trap column (Acclaim PepMap100, 3 µm C18 particle size,
331 100 Å pore size, 75 µm inner diameter, Thermo Fisher Scientific) for 10 min at a flow rate of 6 µl/min with 0.1 % (v/v)
332 TFA as mobile phase. Subsequently, they were separated on a 25 cm long analytical column (Acclaim PepMapRSLC,
333 2 µm C18 particle size, 100 Å pore size, 75 µm inner diameter, Thermo Fisher Scientific) at 60°C using a 2 h gradient
334 from 4 to 40% solvent B (solvent A: 0.1% (v/v) formic acid in water, solvent B: 0.1% (v/v) formic acid, 84% (v/v)
335 acetonitrile in water) at a flow rate of 300 nl / min.

336 Separated Peptides were injected with distal coated SilicaTip emitters (New Objective, Woburn, MA, USA) into an
337 Orbitrap Elite mass spectrometer via a nanosource electrospray interface. The mass spectrometer was operated in
338 positive, data dependent mode with a spray voltage of 1.4 kV and capillary temperature of 275°C. First, a full scan from
339 m/z 350 to 1700 was recorded with a resolution of 60000 (at 400 m/z) in the obitrap analyser with a target for automatic
340 gain control set to 1000000 and a maximal ion time of 200 ms. Then, up to 20 two- and threefold charged precursor
341 ions with a minimal signal of 500 were isolated (isolation width 2) in the linar ion trap part of the instrument. Here, ions

342 were collected for a maximum of 50 ms with an automatic gain control set to 30000, fragmented by collision induced
343 dissociation with a normalized collision energy of 35 and analysed at a resolution of 5,400 (at 400 m/z). Already
344 fragmented precursors were excluded from fragmentation for the next 45 seconds.

345 Quantitative analysis of MS1 based precursor ions was carried out with Progenesis QI for proteomics (version 2.0,
346 Nonlinear Dynamics, Newcastle upon Tyne, UK). The software first detects and aligns precursor ion signals (features)
347 then associates information from MS2 based precursor identification and finally computes protein intensities on basis
348 of associated features. Automatic processing was used without manual alignment adjustment. Here, one run of the
349 control-vector + ME49 could not automatically aligned and was not further considered in the analysis. Searches were
350 triggered by Proteome Discoverer (version 1.4.1.14, Thermo Scientific) and the percolator node was used for
351 identification validation at 1% false discovery rate. Spectra were searched with the Mascot search engine (version
352 MASCOT 2.4.1, Matrix Science, London, UK) considering cysteine carbamidomethylation as fixed and protein N-
353 terminal acetylation and methionine oxidation as variable modification as well as tryptic cleavage specificity with a
354 maximum of two missed cleavage sites. Mass precision was set to 10 ppm for precursor and 0.4 Da for fragment
355 spectra. Database searches were carried out using the mus musculus (UP000000589) and toxoplasma gondii
356 (UP000002226) reference proteome data sets downloaded on 18th January 2018 from UniProtKB including 52548
357 respectively 8404 entries. Only "high confident" peptide spectrum matches were used for further processing and peptide
358 spectrum matches associated with proteins identified with at least two unique peptides. As we noticed a bias towards
359 higher protein intensities in the mGBP2 overexpressing cells (arising from mGBP2 and associated proteins), no global
360 normalization was performed but a normalization of protein intensities based on the sum of the Ig heavy chain proteins
361 P18525, P18524. Calculated protein intensities were further processed within the Perseus (version 1.6.2.2, MPI for
362 Biochemistry, Planegg, Germany) software environment. Here, Student's t-tests were calculated on log2 transformed
363 normalized intensities using the significance analysis of microarrays method for cutoff determination (S_0 set to 0.8, 5%
364 false discovery rate, a minimum of 4 valid values per group). The mass spectrometry proteomics data have been
365 deposited to the ProteomeXchange Consortium via the PRIDE(105) partner repository with the dataset identifier
366 PXD027029.

367 *Immunofluorescence analysis.*

368 Cells were fixed in 4% paraformaldehyde (PFA, Sigma-Aldrich, Germany) permeabilized with 0.02% saponin
369 (Calbiochem-Merck) and blocked in 0.002% saponin with 2% goat serum (DaKoCytomation, Denmark). The outer
370 membrane of T. gondii was visualized by anti-SAG1 (Abcam, UK) at a concentration of 1/700. As secondary reagents,
371 1/200 concentrated Alexa Fluor™ 633-conjugated goat anti-mouse IgG (H+L) (Invitrogen, ThermoFisher Scientific,
372 USA) and Cy3-conjugated goat anti-mouse IgG plus IgM (Jackson ImmunoResearch Laboratories, UK) were used.
373 Nuclei were counterstained with 1/2500 4',6-diamidino-2-phenylindole (DAPI, Invitrogen, ThermoFisher Scientific,
374 USA). The cover slips were fixed in fluorescence mounting medium (Fluoromount-G, Southern Biotechnology
375 Associates, Birmingham, AL). Fluorescence was visualized using a LSM780 confocal microscope (Zeiss, Germany).
376 Image analysis and processing was performed with the ZEN (Zeiss, Switzerland) software.

377 *Gated Stimulated Emission Depletion measurement*

378 Gated Stimulated Emission Depletion (STED) measurements were performed using a TCS SP8 STED 3X (Leica,
379 Wetzlar, Germany) equipped with an HC PL APO CS2 93x glycerol objective (Leica, Wetzlar, Germany, NA 1.3) at a
380 scan speed of 1400 Hz. For the acquisition of the gated STED signal of the eGFPBoosterAtto488, 488 nm was used
381 as the excitation laser line, 592 nm as the corresponding depletion laser line and the hybrid detector range was set
382 from 498 nm to 580 nm with a 1 ns to 6 ns time gating. For the acquisition of the gated STED signal of the
383 mRFPBoosterAtto647N, 633 nm was used as the excitation laser line, 755 nm as the corresponding pulsed depletion
384 laser line and the hybrid detector range was set from 640 nm to 750 nm with a 0.8 ns to 6 ns time gating. Detection of
385 the different signals was carried out in a frame sequential measurement setup. Deconvolved data of gated STED
386 measurements were calculated using Huygens software (Huygens professional, Scientific Volume Imaging,
387 Netherlands) with reduced signal to noise factor of 5 for eGFPBoosterAtto488 and 6 for mRFPBoosterAtto647N and a
388 reduced iteration setting of 20 for both channels. Resulting deconvolved images were visually compared to the raw data
389 to ensure the quality of the calculation. To correct for channel shift, a reference double staining of nuclear pores was
390 acquired with similar settings and utilized as a reference for channel shift correction by the Fiji-plugin “multistackreg”
391 (106).

392 *CRISPR/Cas9 knock out strategy.*

393 The Galectin 9 gene (lectin, galactose binding, soluble 9, Lgls9) as well the Ckap4 gene (P63; CLIMP-63;
394 5630400A09Rik) were disrupted by applying the CRISPR/Cas9 technology in NIH 3T3 fibroblasts (107). The knock out
395 was performed by transfection of the pSpCas9(BB)-2A-GFP (PX458) plasmid (Addgene, USA), expressing a sgRNA
396 (Ckap4: for CAC CGA TCC GCG CCG CCC GAC GGG T, rev AAA CAC CCG TCG GGC GGC GCG GAT C, Gal9: for
397 CAC CGC GGG TTA ATG TAT GGA GAC T, rev AAA CAG TCT CCA TAC ATT AAC CCG C) corresponding to the
398 sequence contained in the first exon of either Gal9 or Ckap4 gene. The sgRNA encoding plasmids were transfected
399 into NIH 3T3 fibroblasts according to jetPRIME^{R} transfection protocol (Polyplus, New York City). The transfection
400 efficacy was analyzed by flow cytometry. Subsequently, GFP positive cells were sorted and single cell colonies were
401 cultivated. Mutated clones of the Gal9 gene were identified by Surveyor® Mutation Detection (Integrated DNA
402 Technologies, Inc., USA) (for AAC TAG ATT GGG CCT GCC TC, rev AGA GAT CCC CCT GAC TCT GT, expected
403 fragments, expected PCR fragment: 923 bp, expected digested fragments: 747, 176 bp). The knock out of both genes,
404 respectively, was confirmed by PCR amplification, subcloning and sequencing of the corresponding gene stretches
405 from different single cell colonies. Additionally, WB analysis was performed with a polyclonal rabbit anti-mouse antibody
406 against Ckap4 (STJ110088, St John's Laboratory Ltd, UK) and a polyclonal rabbit anti-mouse antibody against Gal9
407 (ARP54821_P050, Aviva Systems Biology).

408 **Acknowledgements**

409 We thank Julia Mock, Nicole Küpper and Karin Buchholz for excellent technical assistance. We would like to
410 acknowledge the Center for Advanced Imaging (CAi) at Heinrich Heine University for providing access to the Leica TCS
411 SP8 gSTED 3X microscope system (DFG INST 208/665-1 FUGG). This work was funded by the Deutsche
412 Forschungsgemeinschaft (DFG, German Research Foundation) – Project-ID 233613836 to KP and DD, and Project-ID
413 267205415 – SFB 1208, Z02 to SWP and SH., and by the Jürgen Manchot foundation to KP.

414

415 **References**

416 1. McNab F, Mayer-Barber K, Sher A, Wack A, & O'Garra A (2015) Type I interferons in infectious
417 disease. *Nat Rev Immunol* 15(2):87-103.
418 2. Kak G, Raza M, & Tiwari BK (2018) Interferon-gamma (IFN-gamma): Exploring its implications in
419 infectious diseases. *Biomol Concepts* 9(1):64-79.
420 3. Boehm U, Klamp T, Groot M, & Howard JC (1997) Cellular responses to interferon-gamma.
421 *Annual Review of Immunology* 15:749-795.
422 4. Boehm U*, et al.* (1998) Two families of GTPases dominate the complex cellular response to IFN-
423 gamma. *J.Immunol.* 161(12):6715-6723.
424 5. Martens S & Howard J (2006) The interferon-inducible GTPases. *Annual review of cell and*
425 *developmental biology* 22:559-589.
426 6. Howard JC (2007) Introduction: cell-autonomous immunity. *Microbes Infect* 9(14-15):1633-1635.
427 7. MacMicking JD (2012) Interferon-inducible effector mechanisms in cell-autonomous immunity.
428 *Nature Reviews Immunology* 12(5):367-382.
429 8. Praefcke GJK*, et al.* (2004) Identification of residues in the human guanylate-binding protein 1
430 critical for nucleotide binding and cooperative GTP hydrolysis. *Journal of Molecular Biology*
431 344(1):257-269.
432 9. Praefcke GJK (2018) Regulation of innate immune functions by guanylate-binding proteins. *Int J*
433 *Med Microbiol* 308(1):237-245.
434 10. Zhao YO*, et al.* (2009) Toxoplasma gondii and the immunity-related GTPase (IRG) resistance
435 system in mice - A Review. *Memorias do Instituto Oswaldo Cruz* 104(2):234-240.
436 11. Hunn JP, Feng CG, Sher A, & Howard JC (2011) The immunity-related GTPases in mammals: a
437 fast-evolving cell-autonomous resistance system against intracellular pathogens. *Mamm*
438 *Genome* 22(1-2):43-54.
439 12. Cheng YS, Colonno RJ, & Yin FH (1983) Interferon induction of fibroblast proteins with guanylate
440 binding activity. *J.Biol.Chem.* 258(12):7746-7750.
441 13. Olszewski MA, Gray J, & Vestal DJ (2006) In silico genomic analysis of the human and murine
442 guanylate-binding protein (GBP) gene clusters. *Journal of Interferon and Cytokine Research*
443 26(5):328-352.
444 14. Tripal P*, et al.* (2007) Unique features of different members of the human guanylate-binding
445 protein family. *Journal of Interferon and Cytokine Research* 27(1):44-52.
446 15. Guenzi E*, et al.* (2001) The helical domain of GBP-1 mediates the inhibition of endothelial cell
447 proliferation by inflammatory cytokines. *EMBO J* 20(20):5568-5577.
448 16. Degrandi D*, et al.* (2007) Extensive characterization of IFN-induced GTPases mGBP1 to mGBP10
449 involved in host defense. *Journal of Immunology* 179(11):7729-7740.
450 17. Capaldo CT*, et al.* (2012) IFN-gamma and TNF-alpha-induced GBP-1 inhibits epithelial cell
451 proliferation through suppression of beta-catenin/TCF signaling. *Mucosal Immunol* 5(6):681-690.
452 18. Kim BH, Shenoy AR, Kumar P, Bradfield CJ, & MacMicking JD (2012) IFN-Inducible GTPases in
453 Host Cell Defense. *Cell Host & Microbe* 12(4):432-444.
454 19. Nordmann A, Wixler L, Boergeling Y, Wixler V, & Ludwig S (2012) A new splice variant of the
455 human guanylate-binding protein 3 mediates anti-influenza activity through inhibition of viral
456 transcription and replication. *FASEB journal : official publication of the Federation of American*
457 *Societies for Experimental Biology* 26(3):1290-1300.
458 20. Pilla-Moffett D, Barber MF, Taylor GA, & Coers J (2016) Interferon-Inducible GTPases in Host
459 Resistance, Inflammation and Disease. *J Mol Biol* 428(17):3495-3513.
460 21. Britzen-Laurent N, Herrmann C, Naschberger E, Croner RS, & Sturzl M (2016) Pathophysiological
461 role of guanylate-binding proteins in gastrointestinal diseases. *World J Gastroenterol*
462 22(28):6434-6443.

463 22. Coers J, Brown HM, Hwang S, & Taylor GA (2018) Partners in anti-crime: how interferon-
464 inducible GTPases and autophagy proteins team up in cell-intrinsic host defense. *Current opinion*
465 *in immunology* 54:93-101.
466 23. Ghimire D, Rai M, & Gaur R (2018) Novel host restriction factors implicated in HIV-1 replication. *J*
467 *Gen Virol* 99(4):435-446.
468 24. Honkala AT, Tailor D, & Malhotra SV (2019) Guanylate-Binding Protein 1: An Emerging Target in
469 Inflammation and Cancer. *Front Immunol* 10:3139.
470 25. Steffens N*, et al.* (2020) Essential Role of mGBP7 for Survival of Toxoplasma gondii Infection.
471 *mBio* 11(1).
472 26. Yu P*, et al.* (2020) Guanylate-binding protein 2 orchestrates innate immune responses against
473 murine norovirus and is antagonized by the viral protein NS7. *J Biol Chem* 295(23):8036-8047.
474 27. Praefcke GJK & McMahon HT (2004) The dynamin superfamily: Universal membrane tubulation
475 and fission molecules? *Nature Reviews Molecular Cell Biology* 5(2):133-147.
476 28. Prakash B, Praefcke GJ, Renault L, Wittinghofer A, & Herrmann C (2000) Structure of human
477 guanylate-binding protein 1 representing a unique class of GTP-binding proteins. *Nature*
478 403(6769):567-571.
479 29. Prakash B, Renault L, Praefcke GJK, Herrmann C, & Wittinghofer A (2000) Triphosphate structure
480 of guanylate-binding protein 1 and implications for nucleotide binding and GTPase mechanism.
481 *Embo Journal* 19(17):4555-4564.
482 30. Ghosh A, Praefcke GJK, Renault L, Wittinghofer A, & Herrmann C (2006) How guanylate-binding
483 proteins achieve assembly-stimulated processive cleavage of GTP to GMP. *Nature*
484 440(7080):101-104.
485 31. Kravets E*, et al.* (2012) The GTPase Activity of Murine Guanylate-binding Protein 2 (mGBP2)
486 Controls the Intracellular Localization and Recruitment to the Parasitophorous Vacuole of
487 Toxoplasma gondii. *Journal of Biological Chemistry* 287(33):27452-27466.
488 32. Shydlovskyi S*, et al.* (2017) Nucleotide-dependent farnesyl switch orchestrates polymerization
489 and membrane binding of human guanylate-binding protein 1. *Proc Natl Acad Sci U S A*
490 114(28):E5559-E5568.
491 33. Sistemich L*, et al.* (2020) The Molecular Mechanism of Polymer Formation of Farnesylated
492 Human Guanylate-binding Protein 1. *J Mol Biol* 432(7):2164-2185.
493 34. Virreira Winter S*, et al.* (2011) Determinants of GBP Recruitment to Toxoplasma gondii Vacuoles
494 and the Parasitic Factors That Control It. *Plos One* 6(9).
495 35. Yamamoto M*, et al.* (2012) A Cluster of Interferon-gamma-Inducible p65 GTPases Plays a Critical
496 Role in Host Defense against Toxoplasma gondii. *Immunity* 37(2):302-313.
497 36. Degrandi D*, et al.* (2013) Murine Guanylate Binding Protein 2 (mGBP2) controls Toxoplasma
498 gondii replication. *Proceedings of the National Academy of Sciences of the United States of*
499 *America* 110(1):294-299.
500 37. Selleck EM*, et al.* (2013) Guanylate-binding Protein 1 (Gbp1) Contributes to Cell-autonomous
501 Immunity against Toxoplasma gondii. *Plos Pathogens* 9(4).
502 38. Kravets E*, et al.* (2016) Guanylate binding proteins directly attack Toxoplasma gondii via
503 supramolecular complexes. *Elife* 5.
504 39. Saeij JP & Frickel EM (2017) Exposing Toxoplasma gondii hiding inside the vacuole: a role for
505 GBPs, autophagy and host cell death. *Curr Opin Microbiol* 40:72-80.
506 40. Boothroyd JC (2009) Toxoplasma gondii: 25 years and 25 major advances for the field. *Int J*
507 *Parasitol* 39(8):935-946.
508 41. Sibley LD (2011) Invasion and intracellular survival by protozoan parasites. *Immunological*
509 *reviews* 240(1):72-91.

510 42. Lubitz FP, Degrandi D, Pfeffer K, & Mausberg AK (2013) In Astrocytes the Accumulation of the
511 Immunity-Related GTPases Irga6 and Irgb6 at the Vacuole of Toxoplasma gondii Is Dependent on
512 the Parasite Virulence. *Scientific World Journal*.
513 43. Haldar AK*, et al.* (2013) IRG and GBP host resistance factors target aberrant, "non-self" vacuoles
514 characterized by the missing of "self" IRGM proteins. *PLoS Pathog* 9(6):e1003414.
515 44. Lindenberg V*, et al.* (2017) Broad recruitment of mGBP family members to Chlamydia
516 trachomatis inclusions. *PLoS One* 12(9):e0185273.
517 45. Coers J (2013) Self and non-self discrimination of intracellular membranes by the innate immune
518 system. *PLoS Pathog* 9(9):e1003538.
519 46. Haldar AK*, et al.* (2015) Ubiquitin systems mark pathogen-containing vacuoles as targets for host
520 defense by guanylate binding proteins. *Proceedings of the National Academy of Sciences of the*
521 *United States of America* 112(41):E5628-E5637.
522 47. Fres JM, Muller S, & Praefcke GJK (2010) Purification of the CaaX-modified, dynamin-related
523 large GTPase hGBP1 by coexpression with farnesyltransferase. *Journal of Lipid Research*
524 51(8):2454-2459.
525 48. Liu FT & Rabinovich GA (2010) Galectins: regulators of acute and chronic inflammation. *Annals of*
526 *the New York Academy of Sciences* 1183:158-182.
527 49. Haudek KC*, et al.* (2010) Dynamics of galectin-3 in the nucleus and cytoplasm. *Biochim Biophys*
528 *Acta* 1800(2):181-189.
529 50. Chen HY, Weng IC, Hong MH, & Liu FT (2014) Galectins as bacterial sensors in the host innate
530 response. *Curr Opin Microbiol* 17:75-81.
531 51. Shi W, Xue C, Su XZ, & Lu F (2018) The roles of galectins in parasitic infections. *Acta Trop* 177:97-
532 104.
533 52. Debierre-Grockiego F*, et al.* (2010) Binding of Toxoplasma gondii glycosylphosphatidylinositols to
534 galectin-3 is required for their recognition by macrophages. *J Biol Chem* 285(43):32744-32750.
535 53. Liu FT, Patterson RJ, & Wang JL (2002) Intracellular functions of galectins. *Biochim Biophys Acta*
536 1572(2-3):263-273.
537 54. Cerliani JP, Blidner AG, Toscano MA, Croci DO, & Rabinovich GA (2017) Translating the 'Sugar
538 Code' into Immune and Vascular Signaling Programs. *Trends Biochem Sci* 42(4):255-273.
539 55. Vasta GR (2009) Roles of galectins in infection. *Nat Rev Microbiol* 7(6):424-438.
540 56. Coers J (2017) Sweet host revenge: Galectins and GBPs join forces at broken membranes. *Cell*
541 *Microbiol* 19(12).
542 57. Boyle KB & Randow F (2013) The role of 'eat-me' signals and autophagy cargo receptors in innate
543 immunity. *Curr Opin Microbiol* 16(3):339-348.
544 58. Paz I*, et al.* (2010) Galectin-3, a marker for vacuole lysis by invasive pathogens. *Cell Microbiol*
545 12(4):530-544.
546 59. Casals C, Campanero-Rhodes MA, Garcia-Fojeda B, & Solis D (2018) The Role of Collectins and
547 Galectins in Lung Innate Immune Defense. *Front Immunol* 9:1998.
548 60. Haldar AK, Piro AS, Pilla DM, Yamamoto M, & Coers J (2014) The E2-Like Conjugation Enzyme
549 Atg3 Promotes Binding of IRG and Gbp Proteins to Chlamydia- and Toxoplasma-Containing
550 Vacuoles and Host Resistance. *Plos One* 9(1).
551 61. Thurston TL, Wandel MP, von Muhlinen N, Foeglein A, & Randow F (2012) Galectin 8 targets
552 damaged vesicles for autophagy to defend cells against bacterial invasion. *Nature*
553 482(7385):414-418.
554 62. Feeley EM*, et al.* (2017) Galectin-3 directs antimicrobial guanylate binding proteins to vacuoles
555 furnished with bacterial secretion systems. *Proc Natl Acad Sci U S A* 114(9):E1698-E1706.
556 63. Ling YM*, et al.* (2006) Vacuolar and plasma membrane stripping and autophagic elimination of
557 Toxoplasma gondii in primed effector macrophages. *J.Exp.Med.* 203(9):2063-2071.

558 64. Martens S*, et al.* (2005) Disruption of Toxoplasma gondii parasitophorous vacuoles by the mouse
559 p47-resistance GTPases. *Plos Pathogens* 1(3):187-201.
560 65. Lekutis C, Ferguson DJ, Grigg ME, Camps M, & Boothroyd JC (2001) Surface antigens of
561 Toxoplasma gondii: variations on a theme. *Int J Parasitol* 31(12):1285-1292.
562 66. Mansilla Pareja ME, Bongiovanni A, Lafont F, & Colombo MI (2017) Alterations of the Coxiella
563 burnetii Replicative Vacuole Membrane Integrity and Interplay with the Autophagy Pathway.
564 *Frontiers in cellular and infection microbiology* 7:112.
565 67. Santos JC*, et al.* (2020) Human GBP1 binds LPS to initiate assembly of a caspase-4 activating
566 platform on cytosolic bacteria. *Nat Commun* 11(1):3276.
567 68. Li P*, et al.* (2017) Ubiquitination and degradation of GBPs by a Shigella effector to suppress host
568 defence. *Nature* 551(7680):378-383.
569 69. Pilla DM*, et al.* (2014) Guanylate binding proteins promote caspase-11-dependent pyroptosis in
570 response to cytoplasmic LPS. *Proceedings of the National Academy of Sciences of the United*
571 *States of America* 111(16):6046-6051.
572 70. Creasey EA & Isberg RR (2012) The protein SdhA maintains the integrity of the Legionella-
573 containing vacuole. *Proc Natl Acad Sci U S A* 109(9):3481-3486.
574 71. Meunier E*, et al.* (2014) Caspase-11 activation requires lysis of pathogen-containing vacuoles by
575 IFN-induced GTPases. *Nature* 509(7500):366-+.
576 72. Piro AS*, et al.* (2017) Detection of Cytosolic Shigella flexneri via a C-Terminal Triple-Arginine
577 Motif of GBP1 Inhibits Actin-Based Motility. *mBio* 8(6).
578 73. Ohshima J*, et al.* (2014) Role of Mouse and Human Autophagy Proteins in IFN-gamma-Induced
579 Cell-Autonomous Responses against Toxoplasma gondii. *Journal of Immunology* 192(7):3328-
580 3335.
581 74. Bernardes ES*, et al.* (2006) Toxoplasma gondii infection reveals a novel regulatory role for
582 galectin-3 in the interface of innate and adaptive immunity. *Am J Pathol* 168(6):1910-1920.
583 75. Alves CM*, et al.* (2010) Galectin-3 plays a modulatory role in the life span and activation of
584 murine neutrophils during early Toxoplasma gondii infection. *Immunobiology* 215(6):475-485.
585 76. Schweizer A, Ericsson M, Bachi T, Griffiths G, & Hauri HP (1993) Characterization of a novel 63
586 kDa membrane protein. Implications for the organization of the ER-to-Golgi pathway. *J Cell Sci*
587 104 (Pt 3):671-683.
588 77. Vedrenne C, Klopfenstein DR, & Hauri HP (2005) Phosphorylation controls CLIMP-63-mediated
589 anchoring of the endoplasmic reticulum to microtubules. *Mol Biol Cell* 16(4):1928-1937.
590 78. Kikuchi A, Fumoto K, & Kimura H (2017) The Dickkopf1-cytoskeleton-associated protein 4 axis
591 creates a novel signalling pathway and may represent a molecular target for cancer therapy. *Br J*
592 *Pharmacol* 174(24):4651-4665.
593 79. Gupta N*, et al.* (2006) Identification and characterization of p63 (CKAP4/ERGIC-63/CLIMP-63), a
594 surfactant protein A binding protein, on type II pneumocytes. *American Journal of Physiology-*
595 *Lung Cellular and Molecular Physiology* 291(3):L436-L446.
596 80. Razzaq TM*, et al.* (2003) Functional regulation of tissue plasminogen activator on the surface of
597 vascular smooth muscle cells by the type-II transmembrane protein p63 (CKAP4). *J Biol Chem*
598 278(43):42679-42685.
599 81. Tuffy KM & Lobo Planey S (2012) Cytoskeleton-Associated Protein 4: Functions Beyond the
600 Endoplasmic Reticulum in Physiology and Disease. *International Scholarly Research Notices*
601 10.5402(142313):11.
602 82. Zhang J*, et al.* (2008) Identification of CKAP4/p63 as a major substrate of the palmitoyl
603 acyltransferase DHHC2, a putative tumor suppressor, using a novel proteomics method.
604 *Molecular & cellular proteomics : MCP* 7(7):1378-1388.
605 83. Martin AM, Liu T, Lynn BC, & Sinai AP (2007) The Toxoplasma gondii parasitophorous vacuole
606 membrane: transactions across the border. *J Eukaryot Microbiol* 54(1):25-28.

607 84. Coppens I*, et al.* (2006) Toxoplasma gondii sequesters lysosomes from mammalian hosts in the
608 vacuolar space. *Cell* 125(2):261-274.
609 85. Sehgal A*, et al.* (2005) Peculiarities of host cholesterol transport to the unique intracellular
610 vacuole containing Toxoplasma. *Traffic* 6(12):1125-1141.
611 86. Sibley LD, Niesman IR, Parmley SF, & Cesbron-Delauw MF (1995) Regulated secretion of multi-
612 lamellar vesicles leads to formation of a tubulo-vesicular network in host-cell vacuoles occupied
613 by Toxoplasma gondii. *J Cell Sci* 108 (Pt 4):1669-1677.
614 87. Ridley AJ (2001) Rho proteins: linking signaling with membrane trafficking. *Traffic* 2(5):303-310.
615 88. Kim H, Park M, Kim SJ, & Hwang I (2005) Actin filaments play a critical role in vacuolar trafficking
616 at the Golgi complex in plant cells. *Plant Cell* 17(3):888-902.
617 89. Huang JD*, et al.* (1999) Direct interaction of microtubule- and actin-based transport motors.
618 *Nature* 397(6716):267-270.
619 90. Walker ME*, et al.* (2008) Toxoplasma gondii actively remodels the microtubule network in host
620 cells. *Microbes Infect* 10(14-15):1440-1449.
621 91. Harrison RE*, et al.* (2004) Salmonella impairs RILP recruitment to Rab7 during maturation of
622 invasion vacuoles. *Mol Biol Cell* 15(7):3146-3154.
623 92. Kumar Y & Valdivia RH (2008) Actin and intermediate filaments stabilize the Chlamydia
624 trachomatis vacuole by forming dynamic structural scaffolds. *Cell Host Microbe* 4(2):159-169.
625 93. Youakim A & Ahdieh M (1999) Interferon-gamma decreases barrier function in T84 cells by
626 reducing ZO-1 levels and disrupting apical actin. *Am J Physiol* 276(5):G1279-1288.
627 94. Bromberg JF, Horvath CM, Wen Z, Schreiber RD, & Darnell JE, Jr. (1996) Transcriptionally active
628 Stat1 is required for the antiproliferative effects of both interferon alpha and interferon gamma.
629 *Proc Natl Acad Sci U S A* 93(15):7673-7678.
630 95. Shtrichman R & Samuel CE (2001) The role of gamma interferon in antimicrobial immunity. *Curr*
631 *Opin Microbiol* 4(3):251-259.
632 96. Tong Q*, et al.* (2005) Interferon-gamma inhibits T84 epithelial cell migration by redirecting
633 transcytosis of beta1 integrin from the migrating leading edge. *J Immunol* 175(6):4030-4038.
634 97. Ivanov AI, Parkos CA, & Nusrat A (2010) Cytoskeletal regulation of epithelial barrier function
635 during inflammation. *Am J Pathol* 177(2):512-524.
636 98. Britzen-Laurent N*, et al.* (2013) GBP-1 acts as a tumor suppressor in colorectal cancer cells.
637 *Carcinogenesis* 34(1):153-162.
638 99. Schnoor M, Betanzos A, Weber DA, & Parkos CA (2009) Guanylate-binding protein-1 is expressed
639 at tight junctions of intestinal epithelial cells in response to interferon-gamma and regulates
640 barrier function through effects on apoptosis. *Mucosal Immunol* 2(1):33-42.
641 100. Tietzel I, El-Haibi C, & Carabeo RA (2009) Human guanylate binding proteins potentiate the anti-
642 chlamydia effects of interferon-gamma. *PLoS One* 4(8):e6499.
643 101. Ostler N*, et al.* (2014) Gamma Interferon-Induced Guanylate Binding Protein 1 Is a Novel Actin
644 Cytoskeleton Remodeling Factor. *Molecular and Cellular Biology* 34(2):196-209.
645 102. Meresse S*, et al.* (2001) Remodelling of the actin cytoskeleton is essential for replication of
646 intravacuolar Salmonella. *Cell Microbiol* 3(8):567-577.
647 103. Creasey EA & Isberg RR (2014) Maintenance of vacuole integrity by bacterial pathogens. *Curr*
648 *Opin Microbiol* 17:46-52.
649 104. Grube L*, et al.* (2018) Mining the Secretome of C2C12 Muscle Cells: Data Dependent
650 Experimental Approach To Analyze Protein Secretion Using Label-Free Quantification and
651 Peptide Based Analysis. *J Proteome Res* 17(2):879-890.
652 105. Perez-Riverol Y*, et al.* (2019) The PRIDE database and related tools and resources in 2019:
653 improving support for quantification data. *Nucleic acids research* 47(D1):D442-D450.
654 106. Thevenaz P, Ruttimann UE, & Unser M (1998) A pyramid approach to subpixel registration based
655 on intensity. *IEEE Trans Image Process* 7(1):27-41.

656 107. Ran FA*, et al.* (2013) Genome engineering using the CRISPR-Cas9 system. *Nature protocols*
657 8(11):2281-2308.
658 108. Bollineni RC, Koehler CJ, Gislefoss RE, Anonsen JH, & Thiede B (2018) Large-scale intact
659 glycopeptide identification by Mascot database search. *Sci Rep* 8(1):2117.
660 109. Stratmann B*, et al.* (2016) Glyoxalase 1-knockdown in human aortic endothelial cells - effect on
661 the proteome and endothelial function estimates. *Sci Rep* 6:37737.

662

663

664 **Figures legends**

665 **FIGURE 1. Identification of mGBP2 interacting proteins using co-immunoprecipitation in combination with label-**
666 **free quantitative mass spectrometry.** An HA-mGBP2 fusion protein was expressed in mGBP2$^{-/-}$ MEFs. mGBP2$^{-/-}$ MEFs
667 transduced with the empty expression vector were used as controls. MEFs were stimulated with IFN-γ (16h) and left
668 uninfected or were infected with *T. gondii* ME49 for 2h. IPs were performed with an anti-HA antibody from cell lysates.
669 Immunoprecipitated proteins were analyzed by label-free quantitative mass spectrometry. Five to six replicates were
670 analyzed per condition and putative mGBP2 interacting proteins were identified from uninfected and *T. gondii* ME49 infected
671 cells. Mean values of normalized intensities are shown in the bar plots ± standard deviations. In the table, details from the
672 protein identification are shown: the confidence scores from the MASCOT search engine (108, 109), the number of identified
673 unique peptides per protein as well as p-values from Student's t-tests. Furthermore, the enrichment ratios (intensity ratio
674 between mGBP2 expressing cells and vector control) is given (a correction for multiple testing has been performed using the
675 significance analysis of microarray approach, 5% false discovery rate, S_0 0.8, a minimum of 4 valid values per group).

676 **FIGURE 2. Verification of Gal9 and Ckap4 as interaction partners of mGBP2 by IP analysis.** mGBP2$^{-/-}$ MEFs were
677 reconstituted with GFP-mGBP2 WT or one of the indicated mGBP2 truncation mutants as well as one of the N-terminal
678 mCherry fusion proteins mCherry-mGBP2, mCherry-Gal9 or mCherry-Ckap4. Cells were stimulated with IFN-γ for 16 h
679 and infected with of *T. gondii* ME49 for 4h. Cells were lysed and postnuclear supernatants were incubated o/n with
680 either RFP-Trap® beads or with GFP-Trap® beads at 4°C. IP samples and appropriate cell lysate supernatants were
681 subjected to Western Blotting. Blots were stained with α-GFP or α-mCherry antibodies. GTP-binding domain only (G),
682 the G-domain and the middle domain (GM) or the C-terminal effector domain (E) (36).

683 **FIGURE 3. Intracellular colocalization of mGBP2 interaction partners Gal9 and Ckap4 at the PVM of *T. gondii*.**
684 Recruitment and colocalization of mGBP2, Gal9, and Ckpap4 was analyzed after transduction of a GFP-mGBP2 fusion
685 construct in mGBP2$^{-/-}$ MEFs and additional transduction of either mCherry-Gal9 or mCherry-Ckap4. MEFs were seeded
686 and incubated on glass slides, stimulated with IFN-γ for 16 h and subsequently infected with *T. gondii* ME49 for 2 h.
687 After fixation, infected cells were treated with an α-RFP V_HH nanobody conjugated to eGFPBoosterAtto647N and with
688 an α-GFP V_HH nanobody conjugated to eGFPBoosterAtto488 for enhancement of the immunofluorescence of mCherry
689 and GFP, respectively. Glass slides were analyzed by STED microscopy. Bars 2 µm. The graphs in the right panel
690 depict a fluorescence intensity analysis of STED images on the far right with the ImageJ software (Fiji) for Atto488 and
691 Atto647 fluorescence signals along the cross sections of PVMs as indicated.

692 **FIGURE 4. Gal9 and Ckap4 influence the recruitment of mGBP2 to the PVM of *T. gondii*.** Recruitment of mGBP2
693 to the PVM was analyzed by transduction of a GFP-mGBP2 fusion construct in WT and independent NIH 3T3 cell line
694 clones with verified CRISPR/Cas9 mediated inactivation of Gal9 or Ckap4 (see main text and Figs.S5/S6). Cells were
695 stimulated with IFN-γ for 16 h and subsequently infected with *T. gondii* ME49 for 2 h. The recruitment rate of GFP-
696 mGBP2 in WT cells was set as 100% and the recruitment rate of mGBP2 in the respective knock-out cells was
697 calculated to this reference. The percentage values are plotted on the y-axis. Also, Gal9 and Ckap4 recruitment to the
698 *T. gondii* PV was analyzed in mGBP2$^{-/-}$ vs. WT MEFs transduced either with mCherry-Gal9 or mCherry-Ckap4. The
699 rate of either Gal9 positive or Ckap4 positive PVMs in WT cells was set as 100% and related to the respective rates in
700 mGBP2 knock out cells. The percentage values are plotted on the y-axis. After fixation, *T. gondii* were stained with an
701 α-SAGI antibody and the nuclei were labeled with DAPI. Glass slides were analyzed by confocal microscopy. In each
702 cell line more than 100 PVs were counted. Mean values ± SD are shown.

703 **FIGURE 5. Gal9 and Ckap4 are required for the intracellular control of replication of *T. gondii*.** WT and
704 independent NIH 3T3 cell line clones with verified CRISPR/Cas9 mediated inactivation of Gal9 or Ckap4 (see main text
705 and Figs.S5/S6) were stimulated with IFN-γ for 16 h and subsequently infected with *T. gondii* ME49. After fixation, *T.*
706 *gondii* were stained with an α-SAGI antibody and the cell nuclei were labeled with DAPI. Glass slides were analyzed
707 by confocal microscopy. Bars, 5 µm. The amounts of rosettes (replicative units) and single parasites inside the PV were

708 determined in WT, Gal9- and Ckap4- deficient NIH 3T3 fibroblasts 22 h after infection. In each cell line more than 100
709 PVs were counted. Mean values ± SD are shown (lower panel).

710 **FIGURE 6. Gal9 and Ckap4 control the intracellular replication of *T. gondii*.** WT and independent NIH 3T3 cell line
711 clones with verified CRISPR/Cas9 mediated inactivation of Gal9 or Ckap4 (see main text and Figs.S5/S6) and NIH 3T3
712 cell line clones with verified CRISPR/Cas9 mediated inactivation of Gal9 or Ckap4 reconstituted with mCherry-Gal9 or
713 mCherry-Ckap4 were stimulated with IFN-γ for 16 h and subsequently infected with *T. gondii* ME49 for 22 h. After
714 fixation, *T. gondii* were stained with an α-SAGI antibody and the cell nuclei were labeled with DAPI. Glass slides were
715 analyzed by confocal microscopy. The amounts of rosettes (replicative units) and single parasites inside the PV were
716 determined in WT, Gal9- and Ckap4- deficient and Gal9 or Ckap4 reconstituted NIH 3T3 fibroblasts 22 h after infection.
717 In each cell line more than 100 PVs were counted. Mean values ± SD are shown.

718 **FIGURE S1. Identification of mGBP2 interaction partners.** mGBP2$^{-/-}$ MEFs were reconstituted with HA-mGBP2 or a
719 control vector and stimulated with IFN-γ for 16 h, infected for 2 h with *T. gondii* ME49 or left uninfected. Subsequently,
720 cells were lysed and postnuclear supernatants were incubated o/n with α-HA antibody coupled agarose beads at 4°C
721 for IP. One part of IP samples was separated via 10% SDS-PAGE and labelled using silver staining. Another part of
722 the IP samples was subjected to Western Botting and immune staining with an α-mGBP2 antiserum or an α-HA
723 antibody. A third part of these IP samples was transferred to the MS analysis (see main text).

724 **FIGURE S2. Localization of Gal9 and mGBP2 at *T. gondii*.** Recruitment and colocalization of mGBP2 was analyzed
725 in GFP-mGBP2 expressing mGBP2$^{-/-}$ MEFs with additional transduction of either mCherry-Gal9. MEFs were stimulated
726 with IFN-γ for 16 h and subsequently infected with *T. gondii* ME49 for 5 h. After fixation, *T. gondii* were stained with an
727 α-SAG1 antibody and the cell nuclei were labeled with DAPI. Glass slides were analyzed by confocal microscopy. Bars
728 2 µm.

729 **FIGURE S3. Colocalization of mCherry-mGBP2 and GFP-mGBP2 at the PV membrane of *T. gondii*.** Recruitment
730 and colocalization of mGBP2 was analyzed in GFP-mGBP2 expressing mGBP2$^{-/-}$ MEFs with additional transduction of
731 mCherry-mGBP2 as control. MEFs were stimulated with IFN-γ for 16 h and subsequently infected with *T. gondii* ME49
732 for 2 h. After fixation, *T. gondii* were stained with an α-SAG1 antibody. Infected cells were treated with anti-RFP V_HH

733 nanobody conjugated to eGFPBoosterAtto647N and with anti-GFP V_HH nanobody conjugated to eGFPBoosterAtto488
734 for enhancement of immunofluorescence of mCherry and GFP respectively. Glass slides were analyzed by STED
735 microscopy. Bars 2 µm. The graphs depict a colocalization analysis of STED images with the ImageJ software (Fiji) for
736 GFP and mCherry fluorescence.

737 **FIGURE S4. Intracellular colocalization of mGBP2 with the interaction partners Gal9 and Ckap4**. Colocalization
738 of GFP-mGBP2 with mCherry-Gal9 or mCherry-Ckap4 was analyzed in mGBP2$^{-/-}$ MEFs reconstituted with the indicated
739 fusion proteins. Cells were stimulated with IFN-γ for 16 h. After fixation, cell nuclei were labeled with DAPI. Glass slides
740 were analyzed by confocal microscopy. Bars 5 µm. The right column depicts the results for a colocalization analysis
741 using the Image Visualization and Analysis Software (Imaris) for GFP and mCherry fluorescence.

742 **FIGURE S5. CRISPR/Cas9 gene editing of Gal9 and verification of Gal9 inactivation.** (A) CRISPR/Cas9 and
743 sgRNA specific for Gal9 were expressed in NIH 3T3 fibroblasts. Clones were picked and DNA from WT and three
744 CRIPR/Cas9 Gal9 targeted cell clones of NIH 3T3 fibroblasts was isolated, PCR amplified (923 bp). PCR products were
745 cloned into the pCR2.1 TA-cloning vector. The Gal9 mutations were verified by Sanger sequencing. Indels, AA
746 sequence and premature stop codons (*) are indicated. (B) For independent mutation analysis, the Surveyor® Mutation
747 Detection Kit for Standard Gel Electrophoresis was employed. Here, a mismatch-specific DNA endonuclease to scan
748 mutations and polymorphisms in heteroduplex DNA is used. PCR amplicons from Gal9 mutant NIH 3T3 clones (test)
749 and WT (reference) DNA were hybridized and the mixtures of hetero- and homo-duplexes were submitted to Surveyor
750 Nuclease digestion. The reference DNA alone, treated similarly, served as a negative control. DNA fragments were
751 analyzed by agarose gel electrophoresis. The formation of new cleavage products, due to the presence of one or more
752 mismatches, is indicated by the presence of additional bands. The relative size of these cleavage products indicates
753 the location of the mismatch or mismatches. (C) Postnuclear supernantants of NIH 3T3 cells from different
754 CRISPR/Cas9 Gal9 sgRNA targeted clones and from WT cells were analyzed by WB. WT cells and one CRISPR/Cas9
755 Gal9 sgRNA targeted clone coexpressing GFP-mGBP2 and mCherry-Gal9 served as controls. Cells were stimulated
756 with IFN-γ for 16 h. Blots were stained with α-Gal9 or α-mCherry antibodies.

757 **FIGURE S6: CRISPR/Cas9 gene editing of Ckap4 and verification of Ckap4 inactivation.** CRISPR/Cas9 and
758 sgRNA specific for Ckap4 were expressed in NIH 3T3 fibroblasts. Postnuclear supernatants of NIH 3T3 cells from
759 different CRISPR/Cas9 Ckap4 sgRNA targeted clones versus WT and CRISPR/Cas9 Gal9 sgRNA targeted clones
760 were analyzed by WB. WT and one CRISPR/Cas9 Ckap4 sgRNA targeted clones coexpressing GFP-mGBP2 and
761 mCherry-Ckap4 served as controls. Cells were stimulated with IFN-γ for 16 h. Blots were stained with α-Ckap4 or α-
762 mCherry antibodies.

763 **FIGURE S7. Inactivation of Gal9 or Ckap4 does not influence infection rates of *T. gondii*.** The infection rates of
764 *T. gondii* ME49 were analyzed in WT and independent NIH 3T3 cell line clones with verified Gal9 or Ckap4 inactivation.
765 Cells were stimulated with IFN-γ for 16 h and subsequently infected with *T. gondii* ME49. After fixation, *T. gondii* were
766 stained with the α-SAGI antibody and the cell nuclei were labeled with DAPI. Glass slides were analyzed by confocal
767 microscopy. Bars, 5 µm. The amounts of parasites per cell were quantified 2 h after infection.

768 **FIGURE S8. Influence of mGBP2 does on the recruitment of Gal9 and Ckap4 to the PVM of *T. gondii*.** WT and
769 mGBP2 deficient MEFs additionally transduced with either with mCherry-Gal9 or mChrry-Ckap4 fusion construct were
770 stimulated with IFN-γ for 16 h and subsequently infected with *T. gondii* ME49 for 2 h. After fixation, *T. gondii* were
771 stained with an α-SAGI antibody and the cell nuclei were labeled with DAPI. Glass slides were analyzed by confocal
772 microscopy. Bars, 5 µm.

773 **FIGURE S9. Gal9 and Ckap4 are required for the intracellular control of replication of *T. gondii*.** WT and
774 independent NIH 3T3 cell line clones with verified CRISPR/Cas9 mediated inactivation of Gal9 or Ckap4 (see main text
775 and Figs.S5/S6) were stimulated with IFN-γ for 16 h and subsequently infected with *T. gondii* ME49 for 22 h. After
776 fixation, *T. gondii* were stained with an α-SAGI antibody and the cell nuclei were labeled with DAPI. Glass slides were
777 analyzed by confocal microscopy. Bars, 5 µm.

778 **FIGURE S10. Schematic view of mGBPs, Gal9, and Ckap4 dynamics and multimerization in *T. gondii* infected**
779 **cells.** For details see Results and Discussion.

780

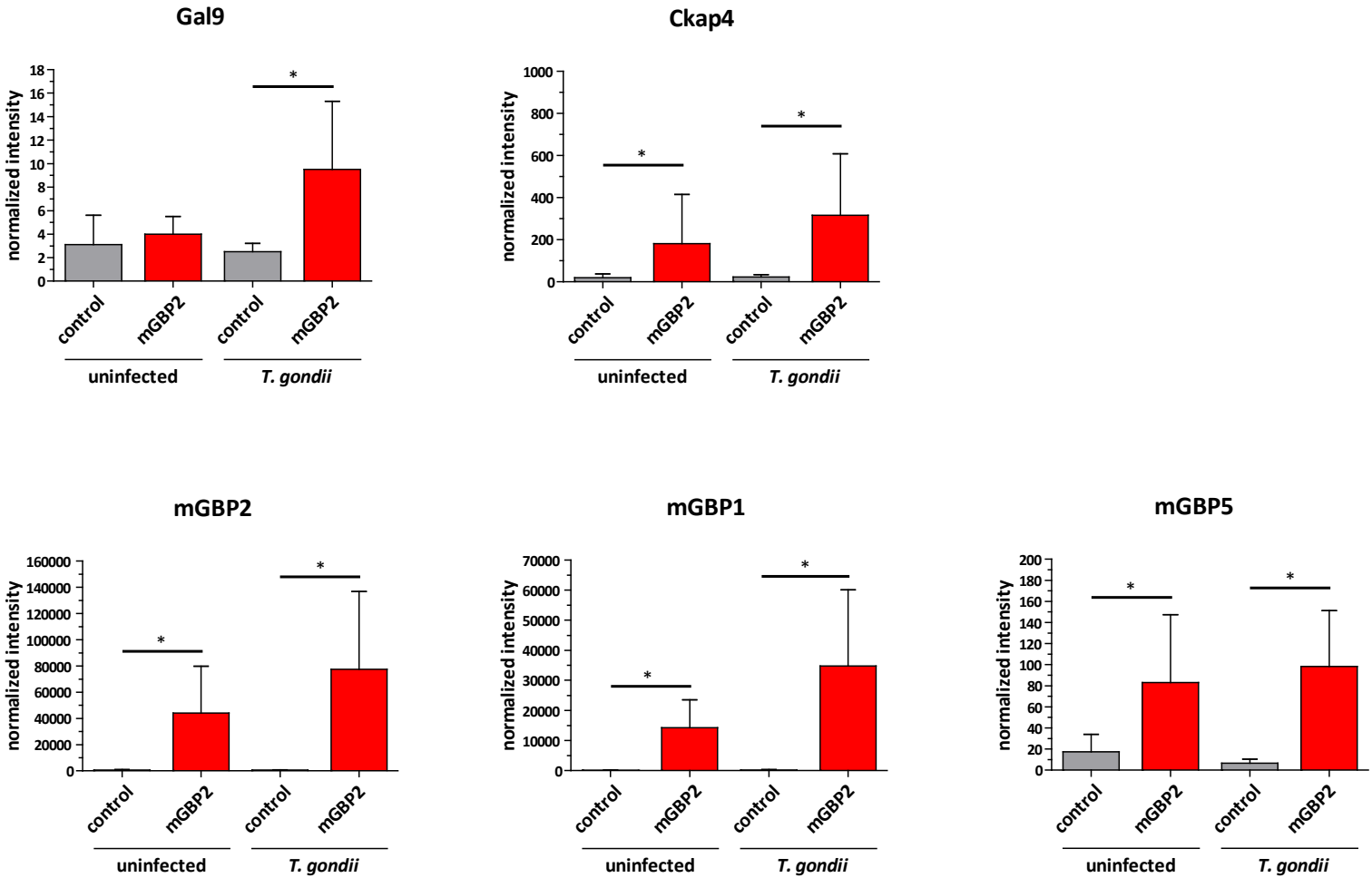

				uninfected			*T. gondii*		
accession	gene names	unique peptides	confidence score	p-value	ratio mGBP2/control	significance mGBP2/control	p-value	ratio mGBP2/control	significance mGBP2/control
Q01514	mGBP1	19	1702.6	3.3E-08	186	+	2.8E-06	199.7	+
Q9Z0E6	mGBP2	55	4193.6	1.3E-07	66.8	+	1.5E-06	125.4	+
Q8CFB4	mGBP5	6	199.1	9.1E-03	4.8	+	6.3E-05	15.1	+
Q8BMK4	Ckap4	13	747.1	1.2E-02	9.2	+	1.0E-02	14	+
O08573	Gal9	2	79.9	1.3E-01	1.5		5.6E-03	3.8	+

Figure 1

IP
RFP trap
16 IFN-γ

mGBP2$^{-/-}$MEFs + *T. gondii* 4 h

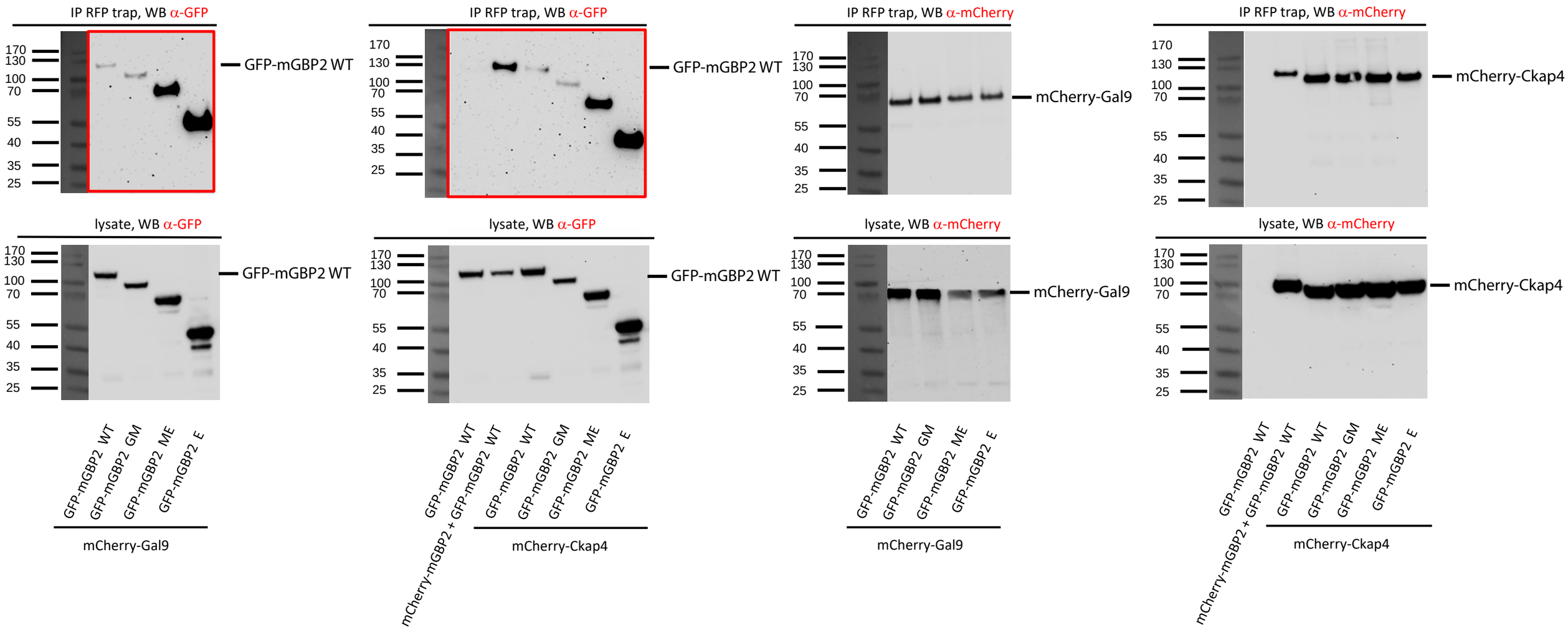

IP
GFP trap
16 IFN-γ

mGBP2$^{-/-}$MEFs + *T. gondii* 4 h

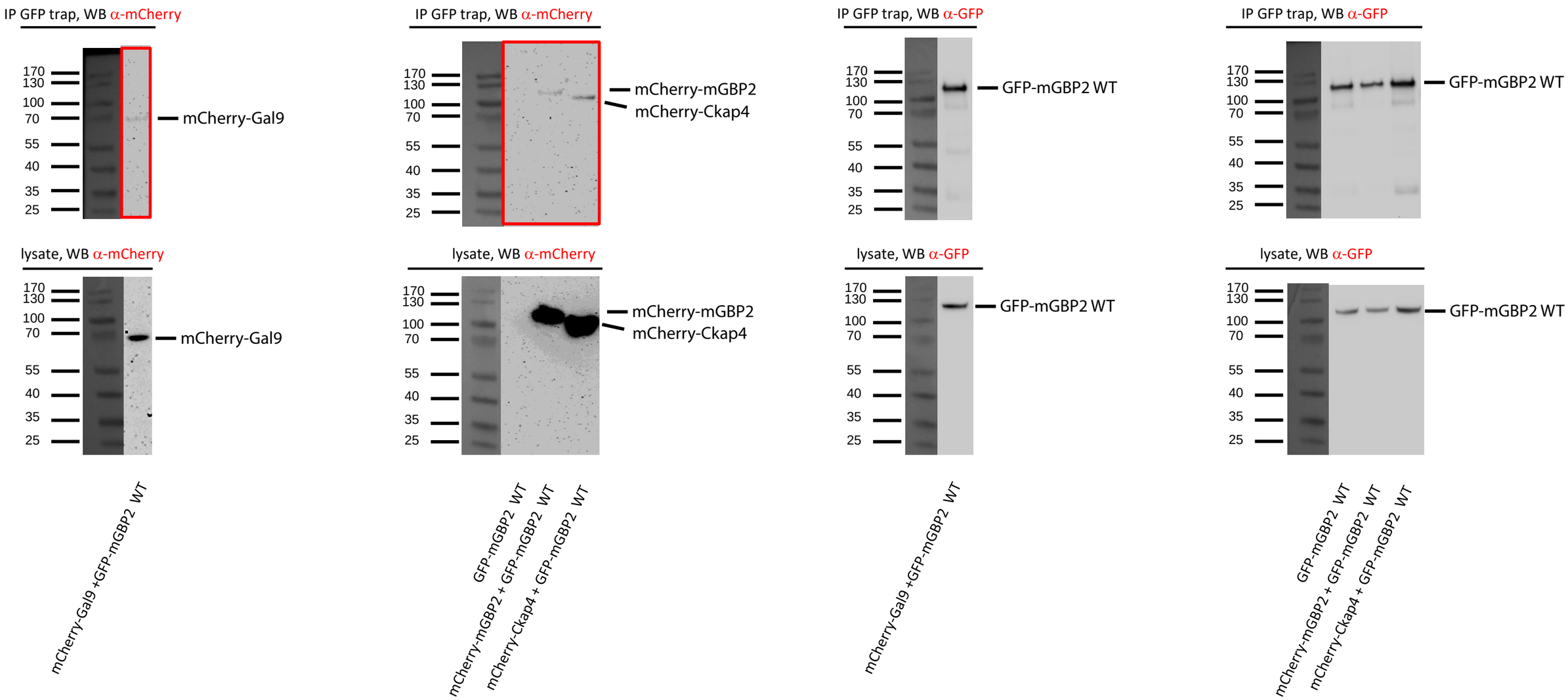

Figure 2

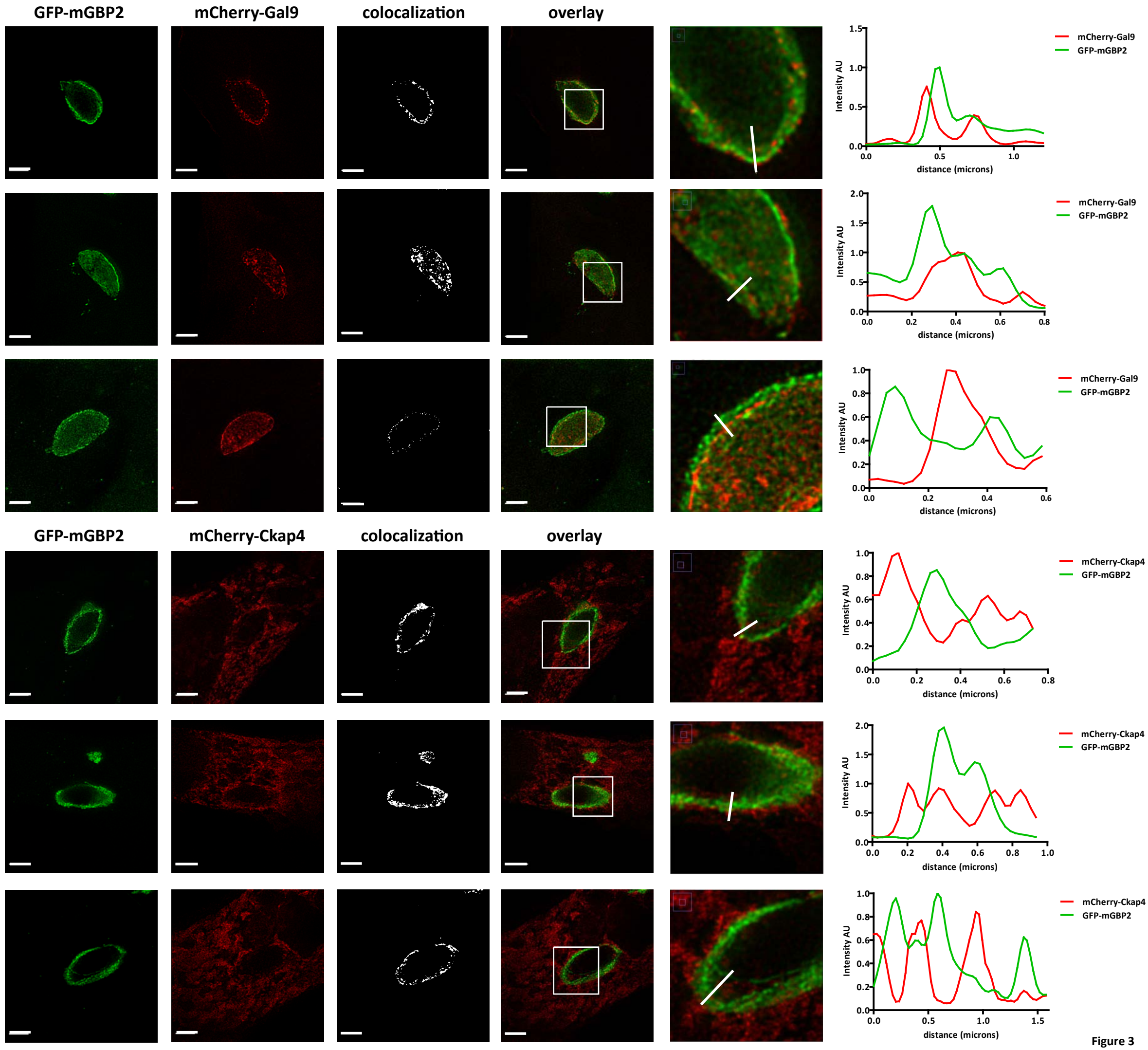
GFP-mGBP2
mCherry-Gal9
colocalization
overlay
mCherry-Gal9
GFP-mGBP2
Intensity AU
distance (microns)
GFP-mGBP2
mCherry-Ckap4
colocalization
overlay
mCherry-Ckap4
GFP-mGBP2
Intensity AU
distance (microns)

Figure 3

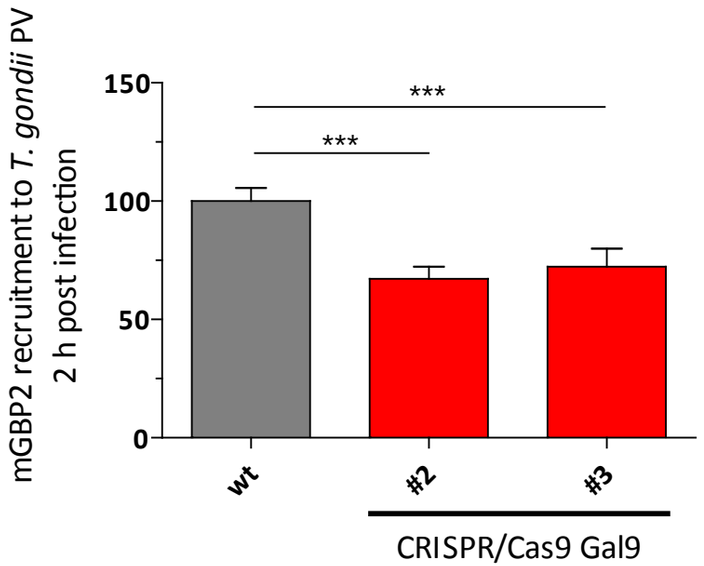
mGBP2 recruitment to T. gondii PV
2 h post infection
150
100
50
0
***
***
wt
#2
#3
CRISPR/Cas9 Gal9

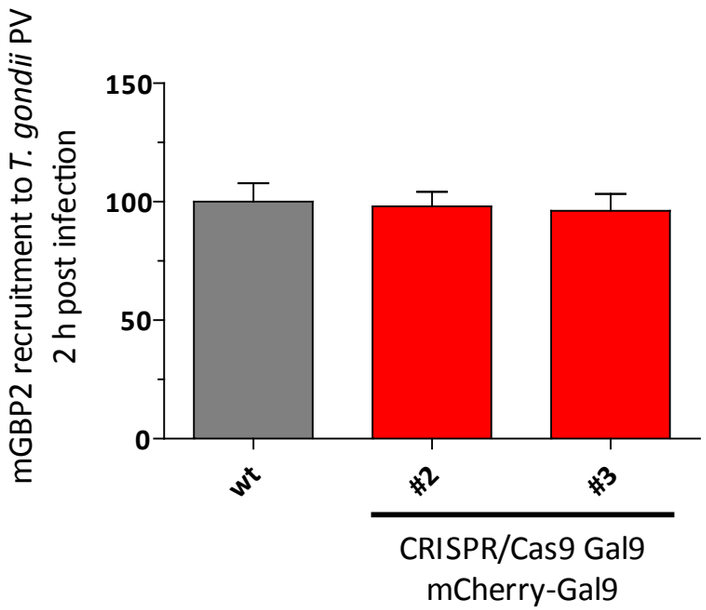
mGBP2 recruitment to T. gondii PV
2 h post infection
150
100
50
0
wt
#2
#3
CRISPR/Cas9 Gal9
mCherry-Gal9

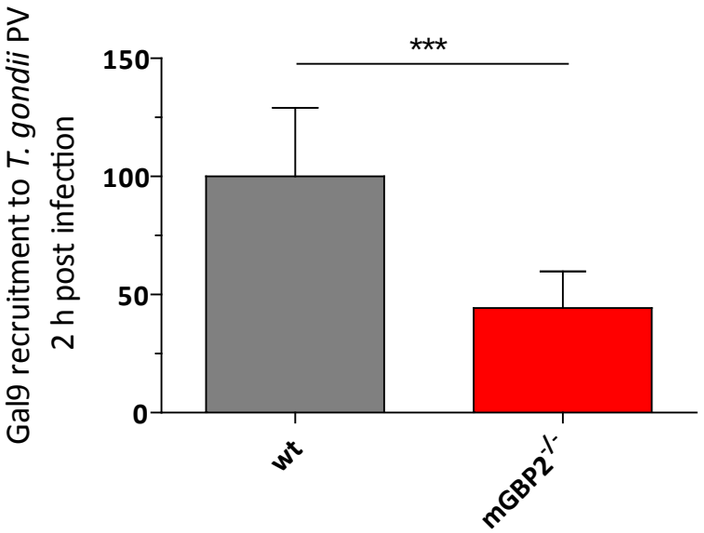
Gal9 recruitment to T. gondii PV
2 h post infection
150
100
50
0
***
wt
mGBP2-/-

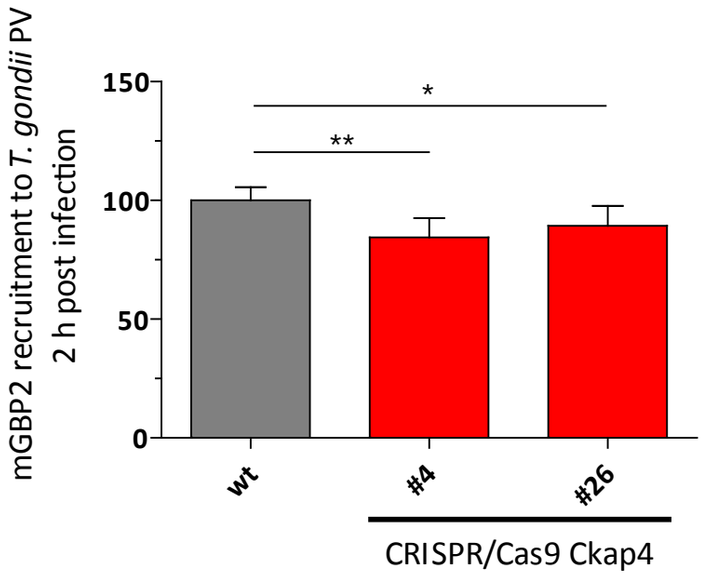
mGBP2 recruitment to T. gondii PV
2 h post infection
150
100
50
0
*
**
wt
#4
#26
CRISPR/Cas9 Ckap4

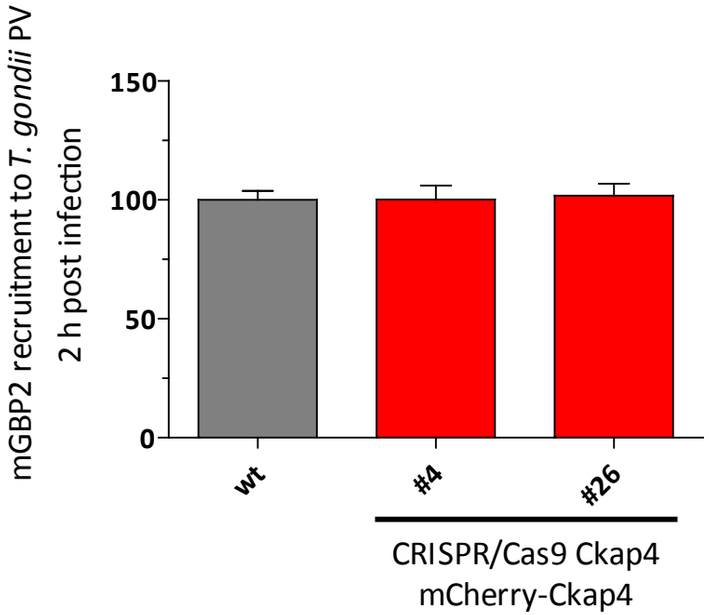
mGBP2 recruitment to T. gondii PV
2 h post infection
150
100
50
0
wt
#4
#26
CRISPR/Cas9 Ckap4
mCherry-Ckap4

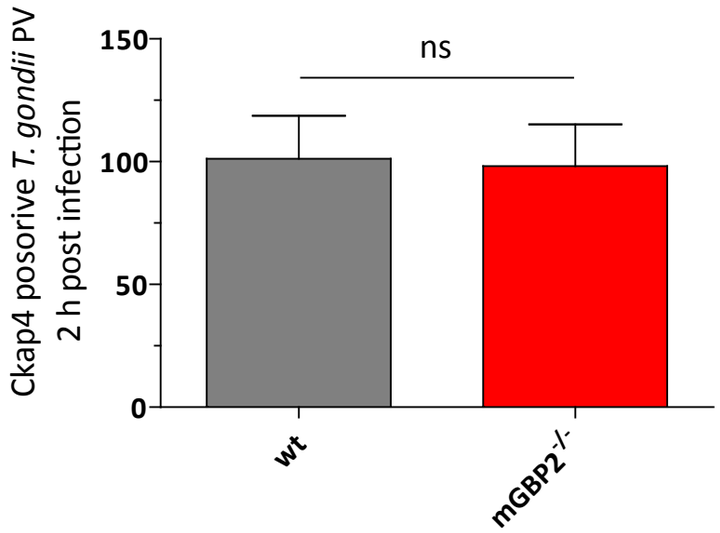
Ckap4 posorive T. gondii PV
2 h post infection
150
100
50
0
ns
wt
mGBP2-/-

Figure 4

CRISPR/Cas9 Gal9 #1

CRISPR/Cas9 Ckap4 #4

T. gondii

T. gondii
DAPI

CRISPR/Cas9 Gal9 #2

CRISPR/Cas9 Ckap4 #26

T. gondii

T. gondii
DAPI

CRISPR/Cas9 Gal9 #3

WT

T. gondii

T. gondii
DAPI

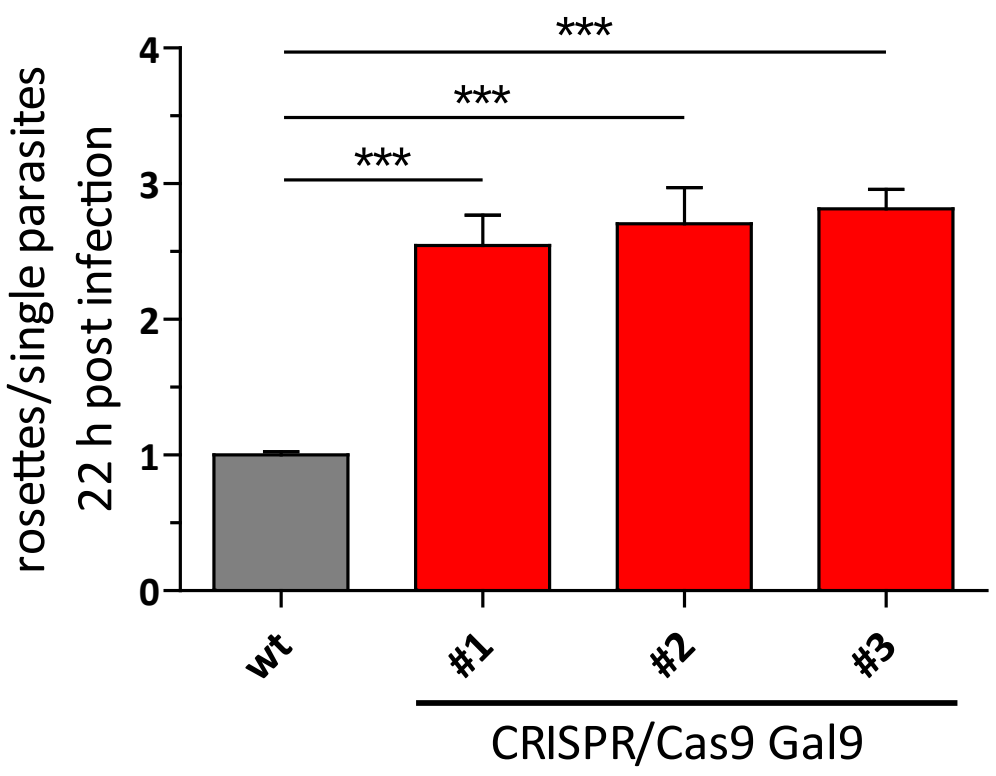

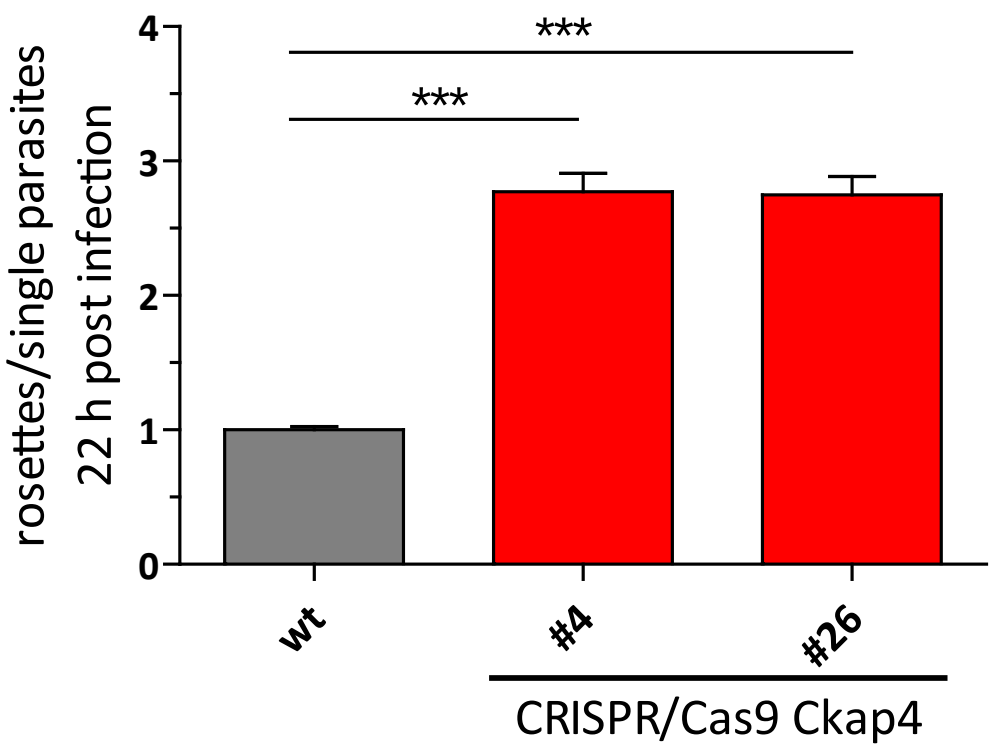

Figure 5

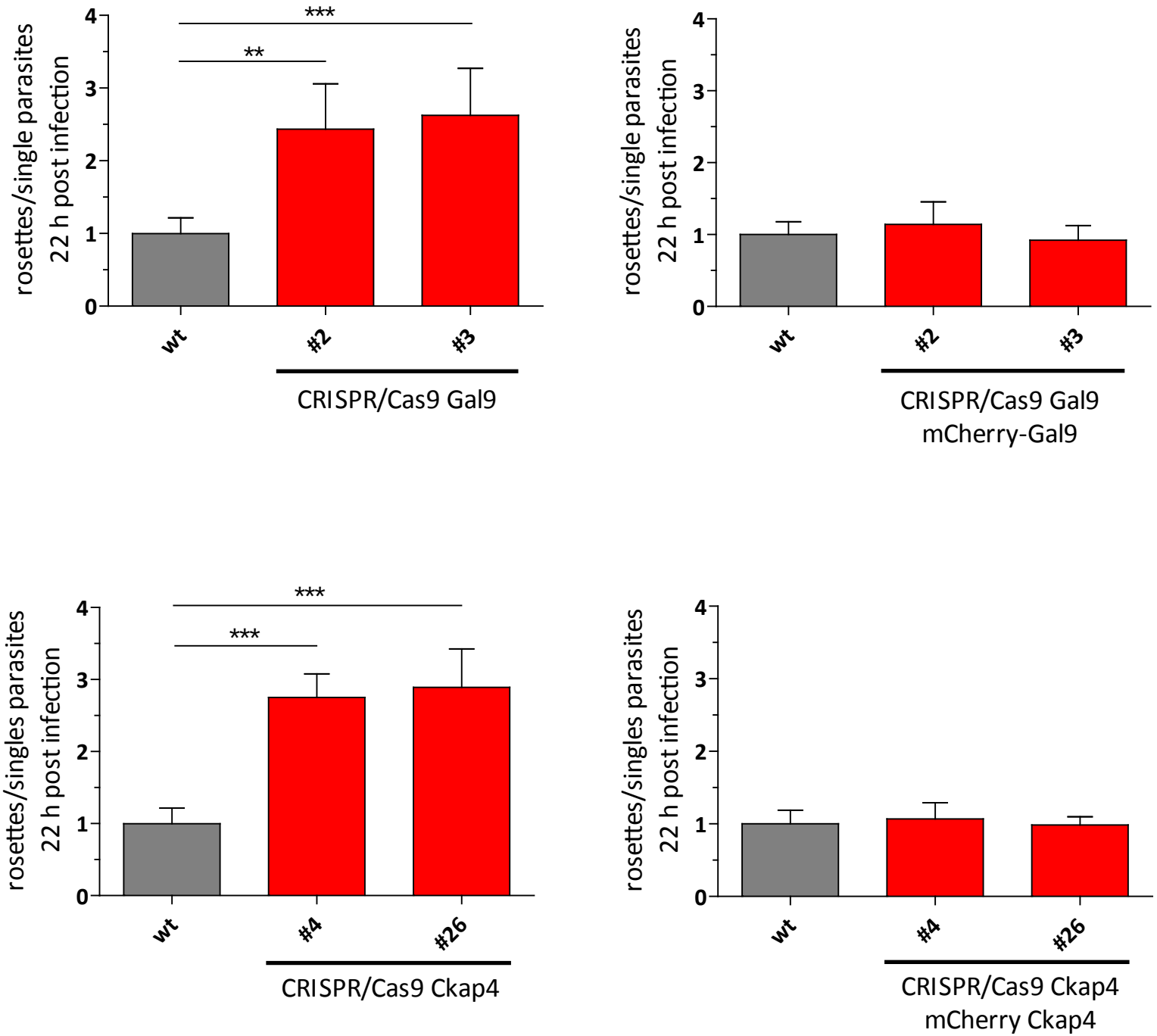
rosettes/single parasites
22 h post infection
4
3
2
1
0
***
**
wt
#2
#3
CRISPR/Cas9 Gal9
rosettes/single parasites
22 h post infection
wt
#2
#3
CRISPR/Cas9 Gal9
mCherry-Gal9
rosettes/singles parasites
22 h post infection
***
***
wt
#4
#26
CRISPR/Cas9 Ckap4
rosettes/singles parasites
22 h post infection
wt
#4
#26
CRISPR/Cas9 Ckap4
mCherry Ckap4

Figure 6